Clim. Past, 11, 803–824, 2015
www.clim-past.net/11/803/2015/
doi:10.5194/cp-11-803-2015

Climate of the Past
Open Access

Bottom water variability in the subtropical northwestern Pacific from 26 kyr BP to present based on Mg / Ca and stable carbon and oxygen isotopes of benthic foraminifera

Y. Kubota[1,2], K. Kimoto[2], T. Itaki[3], Y. Yokoyama[4,5], Y. Miyairi[4], and H. Matsuzaki[6]

[1]Department of Geology and Paleontology, National Museum of Nature and Science, 4-1-1, Amakubo, Tsukuba-shi, Ibaraki 305-0005, Japan
[2]Research Institute for Global Change, Japan Agency for Marine-Earth Science and Technology, 2-15 Natsushima-cho, Yokosuka-shi, Kanagawa 237-0061, Japan
[3]Geological Survey of Japan, National Institute of Advanced Industrial Science and Technology, Central 7, Higashi 1-1-1, Tsukuba-shi, Ibaraki 305-8567, Japan
[4]Atmosphere and Ocean Research Institute, the University of Tokyo, 5-1-5, Kashiwanoha, Kashiwa-shi, Chiba 277-8564, Japan
[5]Department of Biogeochemistry, Japan Agency for Marine-Earth Science and Technology, 2-15, Natsushima-cho, Yokosuka-shi, Kanagawa 237-0061, Japan
[6]Department of Nuclear Engineering and Management, the University of Tokyo, 2-11-16 Yayoi, Bunkyo-ku, Tokyo 113-0032, Japan

Correspondence to: Y. Kubota (yoshimi@kahaku.go.jp)

Received: 27 February 2014 – Published in Clim. Past Discuss.: 28 March 2014
Revised: 18 February 2015 – Accepted: 26 Febrauary 2015 – Published: 3 June 2015

Abstract. To understand bottom water variability in the subtropical northwestern Pacific, bottom water temperatures (BWTs), carbon isotopes ($\delta^{13}C$), and oxygen isotopes of seawater ($\delta^{18}O_w$) at a water depth of 1166 m were reconstructed from 26 kyr BP to present. A new regional Mg / Ca calibration for the benthic foraminifera *Cibicidoides wuellerstorfi* (type B) was established to convert the benthic Mg / Ca value to BWT, based on 26 surface sediment samples and two core-top samples retrieved around Okinawa Island. During the Last Glacial Maximum (LGM), the $\delta^{18}O_w$ in the intermediate water in the northwestern South Pacific was ~ 0.4 ‰ lower than in the deep South Pacific, indicating a greater vertical salinity gradient than at present. This salinity (and probably density) structure would have led to stratification in the intermediate and deep Pacific, which would, in turn, have greatly influenced carbon storage during the glacial time. The benthic Mg / Ca and $\delta^{18}O_w$ records suggest changes that seem to follow Heinrich event 1 (H1) and the Bølling–Alleød (B/A) and Younger Dryas (YD) intervals, with BWT higher during H1 (~ 17 kyr BP) and YD (~ 12 kyr BP) and lower during B/A (~ 14 kyr BP). The warming in the bottom water during H1 suggests increased contribution of North Pacific Intermediate Water (NPIW) to the subtropical northwestern Pacific and decreased upwelling of cooler waters from the abyssal North Pacific. During the interval from 17 to 14.5 kyr BP, the BWT tended to decrease successively in association with a decrease in $\delta^{13}C$ values, presumably as a result of increased upwelling of the abyssal waters to the intermediate depths of the North Pacific caused by shoaling and enhancement of the southward return flow of Pacific Deep Water (PDW). During the Holocene, the millennial- to sub-millennial-scale variations in the BWT generally correlate with the sea surface temperatures in the Okhotsk Sea, the source region of the NPIW, suggesting that changes in the BWT are linked to changes in the NPIW production rate.

1 Introduction

Intermediate and deep water circulation in the Pacific is of particular interest because the deep Pacific is potentially an area in which a large amount of carbon was stored during glacial times (Broecker et al., 2004, 2008). It has been hypothesised that, during the last glacial period, older carbon was released to the atmosphere from the deep Pacific or Southern Ocean through changes in ocean circulation (e.g. Sigman and Boyle, 2000). Thus, the reconstruction of intermediate and deep ocean circulation in the North Pacific and its link to CO_2 release into the atmosphere is essential for understanding of the mechanisms of glacial–interglacial climate change.

At present, deep water formation is absent in the North Pacific because of excess precipitation and subsequent low surface salinity in the subarctic (e.g. Warren, 1983). Instead, the presence of intermediate water in the North Pacific (North Pacific Intermediate Water; NPIW) is seen as a well-defined salinity minimum in the subtropical North Pacific at depths of approximately 300 to 800 m (e.g. Sverdrup et al., 1942; Reid, 1965; Talley, 1993; Yasuda, 1997).

Several studies have been conducted regarding the subarctic Pacific, including the western North Pacific (Ahagon et al., 2003; Sagawa and Ikehara, 2008), the Okhotsk Sea (Ohkushi et al., 2003), and the Bering Sea (Horikawa et al., 2010; Rella et al., 2012). Together, this body of work has improved our understanding of intermediate and deep water formation and ocean circulation in the subarctic North Pacific since the Last Glacial Maximum (LGM). During the LGM, a centre of high-nutrient water, recognised by the lowest benthic carbon isotope values in direction of depth, existed at ∼ 3000 m water depth, which is ∼ 1000–1500 m deeper than the level of a similar layer today in the North Pacific, suggesting a more vertically compressed circulation than today (Keigwin, 1998; Matsumoto et al., 2002). During the last deglaciation, Pacific circulation seemed to shift from a glacial stratified mode to an interglacial upwelling mode during the transition between Heinrich event 1 (H1) and the Bølling–Allerød interval (B/A) (Okazaki et al., 2010, 2012). In particular, deep water formation during H1, which may have reached ∼ 2500 m water depth, was suggested by ^{14}C age differences between planktic and benthic foraminifers (Okazaki et al., 2010). Okazaki et al. (2010) argued that, during H1, a deep Pacific Meridional Overturning Circulation (PMOC) was established, driven by a collapse of the Atlantic Meridional Overturning Circulation (AMOC) that occurred after a large freshwater discharge into the high-latitude North Atlantic. However, recently, Jaccard and Galbraith (2013) argued against such a deep water formation and claimed that waters deeper than ∼ 2400 m were poorly ventilated, while the upper portion of the North Pacific (i.e. above ∼ 1400 m depth) was well ventilated. Regardless of the conclusion of the debate regarding how deep the ventilated water reached during H1, the upper 1400 m of the water column appears to have been well ventilated in the subarctic North Pacific, likely owing to greater NPIW production in association with a shift of its production area from the Okhotsk Sea to the Bering Sea (Rella et al., 2012) or the open subarctic Pacific (Jaccard and Galbraith, 2013). Signs of enhanced ventilation were found off northeastern Japan, suggesting greater lateral advection of NPIW to the mid-latitude northwestern Pacific (Ahagon et al., 2003; Sagawa and Ikehara, 2008). Some of these studies suggested stronger and well-ventilated NPIW also during YD, whereas NPIW during B/A was reduced and less well ventilated. In contrast to the intensive research that has focused on the deglaciation, there are fewer studies dealing with Holocene variability of the intermediate/deep Pacific circulation system.

Investigation of the variability of intermediate water in the subtropical Pacific is significant for our understanding of intermediate/deep ocean circulation in the Pacific as a whole and its links to postulated CO_2 degassing in the South Pacific or Southern Ocean. Nevertheless, the intermediate water variability in the subtropical North Pacific remains poorly understood. To address this, we present intermediate temperature and salinity records based on benthic foraminiferal magnesium / calcium ratios (Mg / Ca) as well as stable oxygen and carbon isotope records that reveal temporal variations in bottom water properties in the northwestern Pacific from 26 kyr BP to present.

2 Oceanographic setting and water mass tracers

The North Pacific can be divided into the subtropical and subarctic gyres at ∼ 35 to 40° N. On the surface, the western boundary current, the Kuroshio, flows northward along the western side of the North Pacific and carries warm, saline, and oligotrophic water to the high latitudes, while the Oyashio flows southward and transports cold and more eutrophic water away from the high latitudes. There are three main water types at intermediate depths (500–1000 m) in the Pacific Ocean: NPIW, Antarctic Intermediate Water (AAIW), and Equatorial Pacific Intermediate Water (EqPIW) (e.g. Bostock et al., 2010). The distribution and flow of NPIW are shown in Fig. 1. NPIW is characterised by low salinity (33.9–34.16) and low oxygen concentrations (50–150 µmol kg^{-1}) (Kaneko et al., 2001; Bostock et al., 2010). At present, this water mass is formed in the Okhotsk Sea, subducts into and below the thermocline of the Kuroshio Extension, enters the subtropical gyres (Reid, 1965; Kaneko et al., 2001), and is distributed at intermediate depths in the North Pacific (Talley, 1993). In the west, a tongue of NPIW extends into the Celebes Sea (Bingham and Lukas, 1995), while in the east, NPIW is restricted to the subtropical gyre by the broad California Current (Talley, 1993). AAIW is a distinctive water mass with high oxygen concentrations (200–250 µmol kg^{-1}) and relatively low salinity (34.3–34.5) (Bostock et al., 2010). AAIW is formed in the southeast Pacific off southern Chile

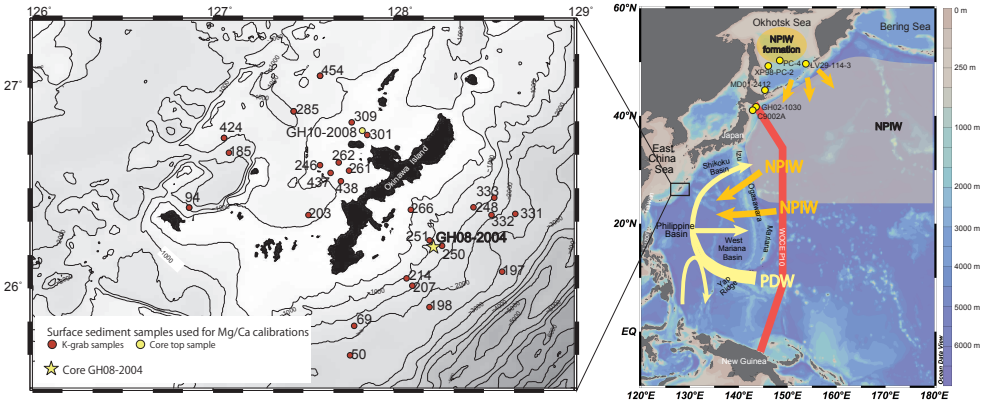

Figure 1. Map showing the locations of surface sediment samples and cores discussed in this study. The orange and yellow arrows indicate the flow of water at 500 and 1500 m water depth, respectively (Kaneko et al., 2001). The red line indicates WOCE Section P10. NPIW: North Pacific Intermediate Water; PDW: Pacific Deep Water.

(Talley, 1996; Tsuchiya and Talley, 1998; Hanawa and Talley, 2001) and flows west into the Coral Sea. The distribution and flow path of AAIW is still under debate (Reid, 1997; Yasuda, 2004; Qu and Lindstrom, 2004). EqPIW is distributed in the equatorial and tropical Pacific (approximately 15° N to 15° S) at intermediate depths (< 1000 m water depth). Based on quasi-conservative tracers, such as radiocarbon ($\Delta^{14}C$), EqPIW is a combination of parental AAIW waters mixed with old PDW. PDW lies beneath the NPIW (< ∼ 1000 m) in the North Pacific (Fig. 2). The deep Pacific is ventilated from the south by the densest waters, such as Antarctic Bottom Water and lower Circumpolar Deep Water, which upwell to moderate depths in the North Pacific and return south as PDW (Schmitz, 1996).

Carbon isotope values ($\delta^{13}C$) of dissolved inorganic carbon (DIC) have been utilised as water mass tracers. The $\delta^{13}C$ values of DIC ($\delta^{13}C_{DIC}$) at intermediate or deep water depths are controlled primarily by the mixing and ages of the water masses, as well as surface water processes such as biological productivity and air–sea exchange (Duplessy et al., 1988; Kroopnick, 1985; Mook et al., 1974). Because lighter ^{12}C is preferentially taken up by phytoplankton to form organic carbon at the surface, $\delta^{13}C_{DIC}$ generally exhibits higher values at the ocean surface. Thus, $\delta^{13}C$ distribution exhibits an inverse relationship with nutrient concentrations. As ^{13}C-depleted organic carbon sinks and remineralises at depth, it decreases the $\delta^{13}C_{DIC}$ of deep water. Modern $\delta^{13}C_{DIC}$ data show a clear separation depending on the water masses, with NPIW (−0.5–0 ‰) < Northern EqPIW (−0.25–0.25 ‰) < Southern EqPIW (0–0.5 ‰) < AAIW (0.75–1.75 ‰) (Bostock et al., 2010). The distribution of the $\delta^{13}C_{DIC}$ is comparable to the phosphate distribution in the North Pacific (Fig. 2). The lowest $\delta^{13}C$ water is found below the main thermocline and above approximately 2500 m water depth (Fig. 2), which is consistent with the highest nutrient content at these depths. Moreover, $\delta^{13}C$ of PDW becomes higher toward the south, which can be explained by mixing with the nutrient-depleted upper Circumpolar Deep Water along the path of its flow (Matsumoto et al., 2002).

The study area is located east of Okinawa Island in the northern part of the Philippine Sea, which lies on the western side of the North Pacific and is composed of three basins: the Shikoku, Philippine, and West Mariana basins (Fig. 1). The general circulation regime changes at around 1500 m water depth in the Philippine Sea (Kaneko et al., 2001). Above this depth, the clockwise subtropical gyre is dominant, with multiple zonal inflows of intermediate waters from western and southwestern areas. NPIW flowing into the Philippine Sea crosses the Izu–Ogasawara–Mariana–Yap Ridge at 26° N, 20° N with a total flow of 11×10^9 kg s^{-1}. Of this, 8×10^9 kg s^{-1} circulates within the subtropical gyre along the Kuroshio, while the remainder is transported to the tropics and the South China Sea (Kaneko et al., 2001). Relatively high-oxygen water does exist in the Okinawa Trough and south of Japan (Komatsu et al., 2004), and had previously been considered to be attributed to the influence of AAIW (Reid, 1997; Yasuda, 2004). However, Qu and Lindstrom (2004) subsequently showed evidence that AAIW does not reach northward of 15° N based on traceable salinity minima. At 1500–3000 m water depth, a main inflow at 9–15° N likely carries PDW from the eastern tropical Pacific along 10° N, forming a large clockwise gyre in the Philippine Basin (Kaneko et al., 2001). The net inflow south of 15° N is estimated to be 17×10^9 kg s^{-1}, all of which returns eastward at 16–24° N (Kaneko et al., 2001). Bottom water $\delta^{13}C_{DIC}$ near site GH08-2004 is −0.19 ‰ at 968 m water depth (Suzuki et al., 2009), which is similar to $\delta^{13}C_{DIC}$ at 10° N at the same depth along 145° E, which is consistent with the postulated flow path. A salinity profile at site GH08-2004 is shown in Fig. 3 (Itaki et al., 2009b) and exhibits a salinity minimum (34.16) that is indicative of the influence of NPIW at 700 m water depth. The increase in salinity deeper than 700 m water

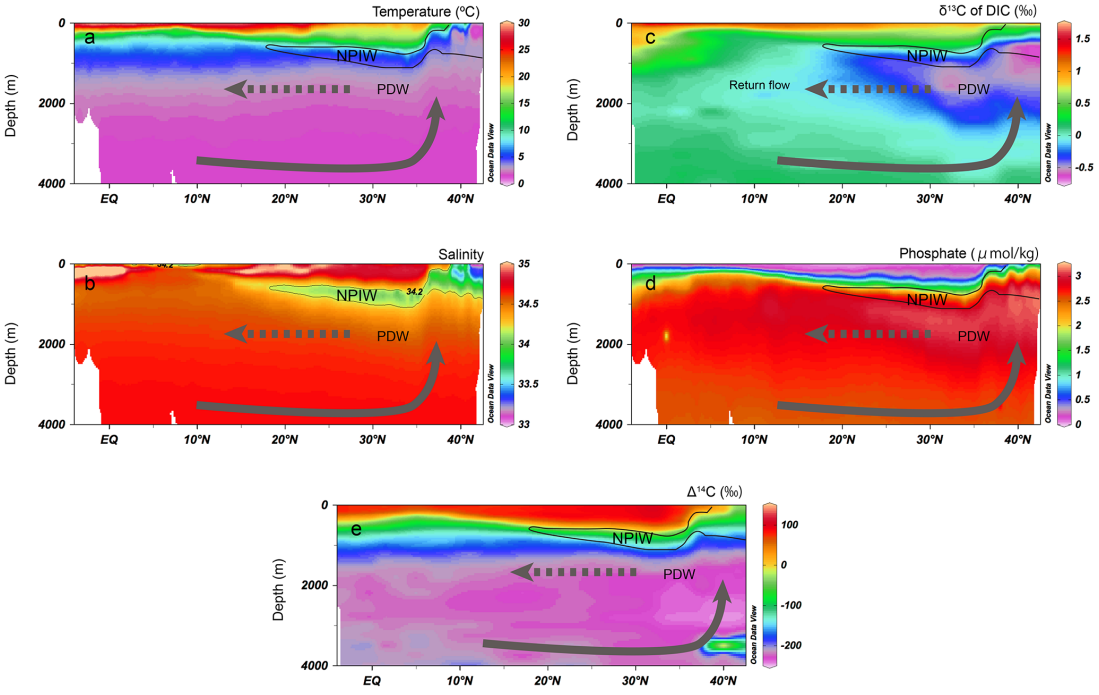

Figure 2. Latitudinal transects along WOCE Section P10: **(a)** temperature, **(b)** salinity, **(c)** δ^{13}C of dissolved inorganic carbon, **(d)** phosphate concentration, and **(e)** Δ^{14}C vs. depth (0–4000 m). All the data from Fukasawa et al. (2005) are available at http://cdiac.ornl.gov/oceans/woce_p10.html. Figures are made with Ocean Data View (Schlitzer, 2009). NPIW: North Pacific Intermediate Water; PDW: Pacific Deep Water. The arrows indicate the upwelling of abyssal Pacific waters and the return flow of PDW.

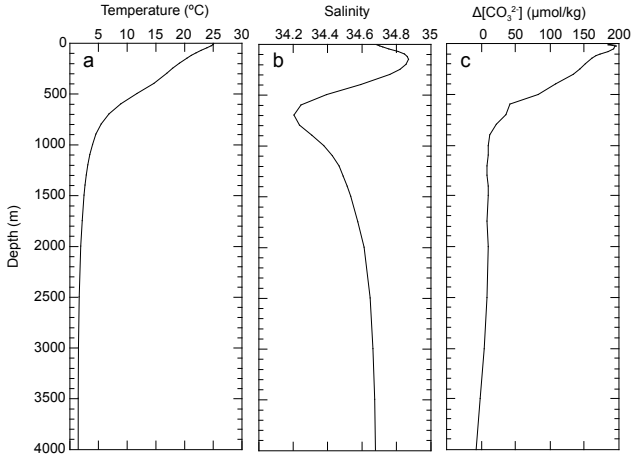

Figure 3. **(a)** Annual temperature and **(b)** salinity profile at World Ocean Atlas Station #664355 (Locarnini et al., 2013; Zweng et al., 2013) and **(c)** $\Delta[CO_3^{2-}]$ at Global Ocean Data Analysis Project (GLODAP) station #28582 (Key et al., 2004).

depth indicates the decreasing contribution of the NPIW and the increasing contribution of relatively more saline PDW. Thus, the bottom at this site is regarded as being primarily under the influence of a mixture of PDW and NPIW.

3 Samples and location

3.1 Surface sediment samples and core GH08-2004

Twenty-six surface sediment samples were recovered from the area around Okinawa Island using a Kinoshita grab sampler (K-grab) during the GH08, GH09, and GH10 cruises of the Geological Survey of Japan on R/V *Hakurei-maru No. 2* (Fig. 1; Itaki et al., 2009a, 2010, 2011a). The samples were collected from a wide range of water depths, from ∼300 to 2700 m. The top 0–2 cm of each of the K-grab samples was taken for the present study. These sediments consisted of sandy mud to mud (Table 1), and the locations of the surface samples were carefully selected and restricted to areas in which reworking or sediment transport from shallower areas (such as turbidites) was unlikely to have occurred. The age uncertainties of the two core-top samples are 347 years for GH08-2004 and 99 years for GH10–2008, respectively, which are extrapolated from the youngest ^{14}C datums (Table 1). Given that the minimum sedimentation rate around Okinawa Island is reported to be ∼5 cm kyr^{-1} (Amano and Itaki, 2012), the maximum age uncertainty for the surface sediment samples is estimated to be ∼400 years. In situ bottom water temperatures (BWTs) and salinities were measured using an Idronaut Ocean Seven 306 conductivity, temperature, and depth (CTD) profiler system attached to the K-grab sampler. These surface sediment samples and two core-

Table 1. List of the surface sediment samples and Mg / Ca values of *C. wuellerstorfi* type B. Mg / Ca variability represents a maximum deviation from the mean value of the measurement.

Sampler	Cruise	Sample ID	Latitude	Longitude	Sample depth (cm)	Description	Water depth (m)	Number of specimens	Bottom water temperature (°C)	Bottom water salinity	$\delta^{18}O_w$ (‰, VSMOW) Suzuki et al. (2010)	$\Delta[CO_3^{2-}]$ (μmol kg^{-1})	Mg / Ca (mmol mol^{-1})	Mg / Ca error ± (mmol mol^{-1})	Equivalent age (yr)
K-grab	GH09	261	N 26°35′15.0"	E 127°45′10.8"	0–2	greyish-olive foraminifer-bearing mud	336	6	16.31	34.71		124.91	3.10		
K-grab	GH09	262	N 26°37′41.4"	E 127°41′44.4"	0–2	olive-yellow mud	346	4	15.89	34.68		122.39	2.6		
K-grab	GH09	301	N 26°45′53.4"	E 127°51′15.0"	0–2	greyish-olive foraminifer-bearing sandy mud	382	9	14.36	34.59		113.32	2.73	0.012	
Gravity core	GH10	GH10–2008 core top	N 26°47′00.6"	E 128°49′04.8"	0–2.2	sandy silt	387	6.00	13.6	34.45		112.06	2.59		99
K-grab	GH09	309	N 26°49′40.2"	E 127°46′0.30"	0–2	olive foraminifer-bearing mud	405	7	13.26	34.53		107.44	2.54	0.076	
K-grab	GH09	438	N 26°32′60.6"	E 127°42′28.8"	0–2	olive-yellow foraminifer-bearing sandy mud	430	5	13.70	34.55		100.76	2.85	0.089	
K-grab	GH09	437	N 26°03′27.6"	E 127°39′01.8"	0–2	olive-yellow mud	446	7	13.06	34.5		96.48	2.55	0.070	
K-grab	GH09	246	N 26°30′41.4"	E 127°35′31.8"	0–2	olive-yellow mud	472	6	12.97	34.52		89.52	2.78		
K-grab	GH08	266	N 26°23′33.6"	E 128°50′43.2"	0–2	greyish-olive mud	496	3	11.92	34.40		83.10	2.10	0.073	
K-grab	GH09	203–2	N 26°21′58.8"	E 127°30′10.2"	0–2	greyish-olive sandy mud	714	7	7.31	34.35		33.71	1.69	0.033	
K-grab	GH09	454	N 27°30′32.4"	E 127°35′33.6"	0–2	olive mud	797	7	6.00	34.39	−0.34	23.08	1.33	0.030	
K-grab	GH10	424	N 26°45′01.2"	E 127°03′39.0"	0–2	dark-olive medium sand (0–1.5 cm) and olive-grey silt (1.5–2 cm)	959	9	4.70	34.41		11.48	1.26	0.028	
K-grab	GH08	251	N 26°14′23.4"	E 128°11′05.4"	0–2	greyish-olive foraminifer-bearing mud	968	8	3.74	34.43		11.20	1.25	0.010	
K-grab	GH09	285	N 26°52′58.2"	E 127°02′40.8"	0–2	olive mud	1008	7	4.81	34.42	−0.38	10.15	1.25	0.051	
K-grab	GH10	94	N 26°24′01.2"	E 126°52′04.2"	0–2	olive silt	1080	4	4.15	34.43		9.98	1.16		
K-grab	GH08	214	N 26°03′00.6"	E 128°04′16.2"	0–2	greyish-olive foraminifer-bearing mud	1117	9	3.17	34.39		9.80	1.05	0.183	
Gravity core	GH08	GH08-2004 core top	N 26°12′51.6"	E 128°14′10.2"	0–2.2	olive mud	1166	7	3.01	34.51		9.82	1.17		347
K-grab	GH10	185	N 26°40′21.6"	E 127°05′12.6"	0–2	greyish-olive sandy silt	1294	8	3.93	34.46		9.26	1.11	0.027	
K-grab	GH08	248	N 26°24′18.6"	E 128°26′30.6"	0–2	dark olive foraminifer-bearing sandy mud	1369	13	2.58	34.54		10.11	1.23	0.045	
K-grab	GH08	250	N 26°12′46.2"	E 128°16′04.8"	0–2	dark greyish-yellow foraminifer-bearing mud	1369	10	2.71	34.54		10.11	0.047		
K-grab	GH08	207	N 26°00′04.8"	E 128°00′37.2"	0–2	greyish-olive foraminifer-bearing mud	1455	11, 10[a]	2.51	34.56		10.67	1.13	0.22[b]	
K-grab	GH08	333	N 26°27′09.6"	E 128°33′25.2"	0–2	yellowish-brown foraminifer-bearing mud	1611	9	2.07	34.51		10.27	0.99	0.050	
K-grab	GH08	69	N 25°48′44.4"	E 127°46′53.4"	0–2	greyish-yellow foraminifer-bearing sandy mud	1774	6	2.17	34.58		9.66	1.05		
K-grab	GH08	332	N 26°22′00.0"	E 128°03′15.0"	0–2	yellowish-brown foraminifer-bearing sandy mud	1952	11	2.09	34.56		10.53	0.85	0.009	
K-grab	GH08	331	N 26°22′20.4"	E 128°40′24.6"	0–2	yellowish-brown foraminifer-bearing mud	2195	4, 2[a]	1.83	34.59		9.98	0.88	0.048[b]	
K-grab	GH08	198	N 25°54′22.2"	E 128°11′53.4"	0–2	greyish-olive foraminifer-bearing sandy mud	2201	2	1.84	34.64		9.95	0.83	0.058	
K-grab	GH08	50	N 25°39′48.6"	E 127°45′29.4"	0–2	greyish-yellow foraminifer-bearing mud	2281	3	1.88	34.63		9.63	0.91		
K-grab	GH08	197	N 26°50′00.6"	E 128°36′01.2"	0–2	greyish-olive foraminifer-bearing mud	2679	6	1.65	34.66		7.27	1.13	0.176	

[a] Foraminiferal tests were repicked and rerun for Mg / Ca analysis. [b] Maximum deviation from the average of the duplicated analyses.

top samples were used to calibrate benthic Mg / Ca to BWT (Table 1). Since CTD measurements were not conducted at the core sites, CTD data from the vicinity were used for BWTs of the core-top samples.

In order to evaluate the influence of carbonate saturation on Mg / Ca values, calcite saturation state in this area was estimated using CO2sys.xls (ver. 12) (Pelletier et al., 2005) with parameters including pressure, BWT (°C), salinity, total CO_2 (μmol kg^{-1}), and alkalinity (μmol kg^{-1}) (Yu and Elderfield, 2008). BWT and salinity data were obtained from World Ocean Atlas station #664355 (Locarnini et al., 2013; Zweng et al., 2013), and total CO_2 (μmol kg^{-1}) and alkalinity (μmol kg^{-1}) were obtained from Global Ocean Data Analysis Project (GLODAP) station #28582 (Key et al., 2004). The equilibrium constants K_1 and K_2 are those from Dickson and Millero (1987), and the dissolution constant K_{SO_4} for the bisulfate ion was obtained from Dickson (1990). Carbonate saturation state was defined as $\Delta[CO_3^{2-}] = [CO_3^{2-}] - [CO_3^{2-}]_{sat}$. $[CO_3^{2-}]_{sat}$ was calculated by $[CO_3^{2-}]_{sat} = [CO_3^{2-}]/\Omega$, where Ω is the solubility ratio of calcite.

A gravity core (GH08-2004, with a length of 2.73 m) was recovered from the continental slope east of Okinawa Island (26°12′52"N, 127°5′13"E; 1166 m water depth). An olive-coloured oxidation layer was identified in the upper 8 cm of the core (Itaki et al., 2009a), while the lower part of the core consisted of olive to grey silty clay with some patches of sand. A brownish-grey tephra layer was recognised at 43 cm beneath the seafloor, and was identified as the K–Ah tephra (7.3 kyr BP; Kitagawa et al., 1995) based on chemical analyses using an electron probe micro-analyser (Itaki et al., 2009a). The core material was subsampled at 2.2 cm intervals, and roughly half of the horizons were processed for measurement. On average, we measured the samples at ∼ 3.6 cm intervals for the stable isotopes and ∼ 4.3 cm for the trace elements.

3.2 Age model for GH08-2004

Radiocarbon analyses (Table 2) were carried out by accelerator mass spectrometry (AMS) on approximately 6–12 mg of the planktic foraminifera *Globigerinoides sacculifer, Globigerinoides ruber, Globorotalia menardii*, and *Globorotalia truncatulinoides* in addition to the results by Itaki (2010) and Itaki et al. (2011b). The foraminiferal tests were extracted from sediment samples in 10 core horizons. The conventional ^{14}C dates were converted to calendar ages using Calib 6.0 software (Stuiver and Reimer, 1993) with the Intcal/Marine09 calibration curve (Reimer et al., 2009). A ΔR value of 44 ± 16 years was used as the regional reservoir correction, derived from six locations in the Ryukyu Islands (Yoneda et al., 2007). The ^{14}C datum just above the K–Ah tephra at 43 cm is in good agreement with the age of the tephra (7.3 kyr BP; Kitagawa et al., 1995) (Fig. 4). Because the ages from deeper-dwelling species (*G. menardii* and *G. truncatulinoides*) are in line with ages interpolated or extrapolated from surface-dwelling species (Fig. 4), it is highly unlikely that mixing these species would give skewed results. This is supported by the fact that an unpublished ^{14}C age of *G. truncatulinoides* from 172.8 to 175.1 cm depth is within the range of 2σ error of the age of the surface-dwelling species (T. Itaki, personal communication, 2014). Ages of GH08-2004 were interpolated between calibrated ^{14}C dates including deeper-dwelling species and the tephra. Linear sedimentation rates were ∼ 10–15 cm kyr^{-1} from 26 to 7.3 kyr BP and ∼ 6–8 cm kyr^{-1} from 7.3 kyr BP to present. The time resolutions achieved were ∼ 340 and ∼ 430 yrs for the isotope and trace element analyses, respectively.

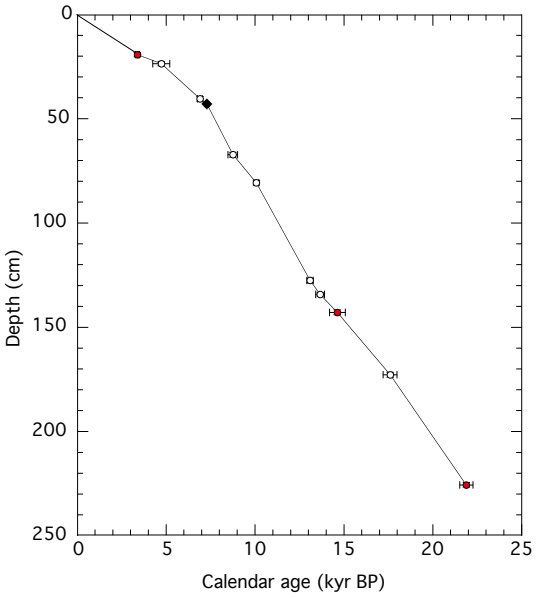

Figure 4. Age model of GH08-2004. Open symbols represent the ^{14}C data and 2σ errors. The filled symbol represents the K–Ah tephra. Red circles indicate ^{14}C ages from deeper-dwelling planktic foraminifers.

3.3 Benthic foraminifera *Cibicidoides wuellerstorfi*

The benthic foraminifera genus *Cibicidoides* is widely used in palaeoceanographic reconstructions because of its epifaunal habitat and wide distribution. Mg / Ca calibration equations have been proposed for several *Cibicidoides* species, such as *C. wuellerstorfi*, *Cibicidoides pachyderma*, and *Cibicidoides compressus* (Rosenthal et al., 1997; Rathburn and De Decker, 1997; Lear et al., 2002; Martin et al., 2002; Elderfield et al., 2006; Marchitto et al., 2007; Healey et al., 2008; Yu and Elderfield, 2008; Raitzsch et al., 2008; Tisserand et al., 2013). Although *C. wuellerstorfi* was recognised in most of the surface sediments used in this study, the other *Cibicidoides* species were rare. *C. wuellerstorfi* observed in this study has two types of surface texture: one is sensu stricto, with a relatively smooth surface texture (type A), while the

Table 2. Radiocarbon data from core GH08-2004.

	Depth (cm)	Species	Conventional ^{14}C age (yr BP)	Error ±	Calendar age (yr BP)	Error ± (1σ)	Error ± (2σ)	Code
Planktic foraminifers	19.3–21.4	*G. menardii*	3530	40	3383	50	118	Beta-260492[a]
	23.6–25.7	*G. sacculifer*	4540	170	4726	226	478	MTC-13738
	40.5–42.7	*G. sacculifer* and *G. ruber*	6450	40	6903	64	135	Beta-293085[b]
	67.3–69.5	*G. sacculifer*	8265	100	8753	148	269	MTC-13739
	80.7–82.9	*G. ruber*	9320	40	10 078	60	135	Beta-344154[a]
	127.6–129.8	*G. ruber*	11 660	50	13 092	75	179	Beta-344155
	134.3–136.0	*G. sacculifer*	12 265	110	13 662	116	249	MTC-13741
	142.9–145.2	*G. truncatulinoides*	12940	70	14 636	235	446	Beta-260494[a]
	172.8–175.1	*G. sacculifer*	14 955	115	17 599	199	390	MTC-13742
	225.6–227.9	*G. truncatulinoides*	18 780	100	21 884	224	371	Beta-260495
Ash layer	43.0	K–Ah			7300			

[a] ^{14}C data from Itaki (2010). [b] ^{14}C data from Itaki et al. (2011b).

other is characterised by a granular surface on the umbilical side (type B) (Fig. 5; see "Taxonomic note" for a detailed description). It is highly unlikely that the granular surface of type B results from secondary calcite deposition based on the SEM images, because *C. wuellerstorfi* type B does not have such a texture on the spiral side (Fig. 5b). *C. wuellerstorfi* type B was more abundant than *C. wuellerstorfi* type A in most of the surface and core samples; therefore, the Mg / Ca temperature calibration equations were generated for type B. *C. wuellerstorfi* type B was used for the oxygen and carbon isotope time series. The oxygen and carbon isotopes of *C. wuellerstorfi* type A were also measured for 28 horizons, but Mg / Ca measurements were not performed owing to inadequate sample sizes.

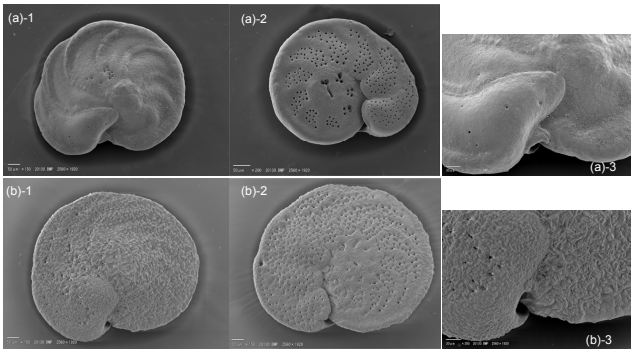

Figure 5. SEM images of *C. wuellerstorfi* type A: sensu stricto **(a)**-1 umbilical side, **(a)**-2 spiral side, **(a)**-3 aperture and *C. wuellerstorfi* type B **(b)**-1 umbilical side, **(b)**-2 spiral side, and **(b)**-3 aperture.

4 Analytical methods

Approximately 10–20 cm^3 of the K-grab and core materials was washed onto a 63 µm mesh sieve and dried in the oven at 50 °C. As many foraminifera tests as possible were picked from each sediment sample, and 1 to 20 well-preserved and clean tests were picked from the > 250 µm size fraction for Mg / Ca and isotope analyses. Cleaning steps based on Boyle and Keigwin (1985) were carried out prior to analyses with some slight modifications (Kubota et al., 2010). All cleaning steps were conducted in a class 10 000 laminar flow clean bench at the Research Institute for Global Change (RIGC), Japan Agency for Marine-Earth Science and Technology (JAMSTEC). First, the foraminiferal tests were crushed on a glass slide and placed into a micro-tube, where they were repeatedly washed using ultra-pure (Milli-Q) water (> 18.3 MΩ) and methanol in an ultrasonic bath. Then, the samples were divided into two micro-tubes, for isotope and Mg / Ca analyses, respectively. For the Mg / Ca samples, additional cleaning steps were conducted; in particular, organic matter and manganese–iron oxides were removed using a reductive and oxidative procedure (Boyle, 1994). For 20 surface sediment samples, the foraminiferal tests were split into several sample cups after the cleaning steps and trace element compositions were measured for each sample cup. The obtained Mg / Ca ranges for each horizon are expressed as error bars in Fig. 6. For two of the surface sediment samples (#331 and #207), another set of the foraminiferal tests was repicked, cleaned, and subjected to trace element analysis (Table 1).

Mg / Ca analysis was performed using a magnetic sector field inductively coupled plasma mass spectrometer (Thermo Finnigan, ELEMENT2) at the Mutsu Institute for Oceanography (MIO), JAMSTEC. Four isotopes of three elements (^{24}Mg, ^{44}Ca, ^{48}Ca, ^{55}Mn) were analysed using Sc as an internal standard. We used the SPEX Claritas PPT certified solutions as standard elemental solutions for all elements. Four working standards were prepared via successive dilutions of the stock standard solutions to match the concentrations of Ca (20 to 5 ppm) and Mg (0.05 to 10 ppb), covering the ranges of the Ca and Mg concentrations found in all of the samples. The precision of replicate analyses of the working standard for Mg / Ca in one sequence was better than ± 0.03 mmol mol^{-1}. Mn / Ca was monitored to

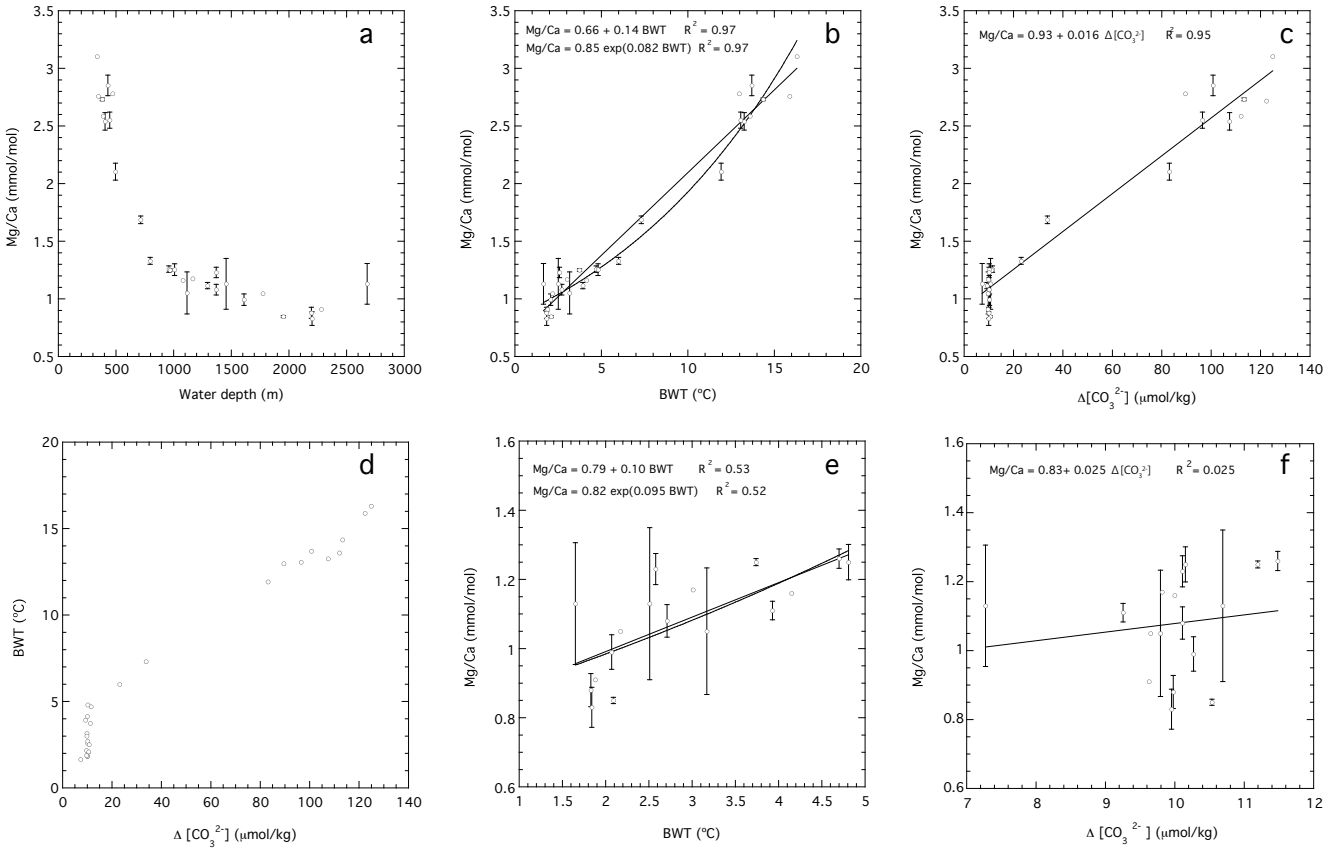

Figure 6. Mg / Ca values of *C. wuellerstorfi* type B from the surface sediment samples vs. **(a)** water depth, **(b)** BWT, and **(c)** $\Delta[CO_3^{2-}]$. **(d)** BWT vs. $\Delta[CO_3^{2-}]$. Mg / Ca values vs. **(e)** BWT, and **(f)** $\Delta[CO_3^{2-}]$ in the low temperature range. All the data are presented in Table 1.

check for possible diagenetic overgrowths (Boyle, 1983). Average Mn / Ca was 88 µmol mol^{-1}, and the standard deviation was found to be ± 326 µmol mol^{-1} (1σ) owing to a few extremely high Mn / Ca values (> 1000 µmol mol^{-1}). Three samples with Mn / Ca values over 1σ were discarded.

δ^{18}O and δ^{13}C of both types of *C. wuellerstorfi* ($\delta^{18}O_c$ and $\delta^{13}C_c$ respectively) were measured using a Finnigan MAT 252 mass spectrometer (IR–MS) with a Kiel III carbonate device at the MIO, JAMSTEC. The reproducibility of the measurements was better than ± 0.05 ‰ (1σ) for both δ^{18}O and δ^{13}C, as determined by replicate measurements of the international standard NBS-19.

5 Results of Mg / Ca calibration

Previous studies have revealed that Mg / Ca of the benthic foraminifera *C. wuellerstorfi* are controlled by both the temperature and carbonate chemistry of seawater, especially at lower $\Delta[CO_3^{2-}]$ (Elderfield et al., 2006; Yu and Elderfield, 2008; Raitzsch et al., 2008; Healey et al., 2008). Here, we compare our benthic Mg / Ca results and their sensitivity to BWT and $\Delta[CO_3^{2-}]$. Raitzsch et al. (2008) argued that Mg / Ca of *C. wuellerstorfi* is more dependent on dissolved inorganic carbon (DIC = $[CO_2]_{aq} + [HCO_3^-] + [CO_3^{2-}]$) than on $\Delta[CO_3^{2-}]$. $\Delta[CO_3^{2-}]$ decreases with decreasing $[CO_3^{2-}]$, while DIC increases with decreasing $[CO_3^{2-}]$. Since both $\Delta[CO_3^{2-}]$ and DIC are linked to $[CO_3^{2-}]$, $\Delta[CO_3^{2-}]$ is employed here to discuss the influence of carbonate chemistry.

Mg / Ca values of *C. wuellerstorfi* type B obtained from the 28 surface sediment samples range from 0.83 to 3.10 mmol mol^{-1} and decrease rapidly with depth to ∼ 1000 m water depth, owing to the steeper gradient of the BWT and $\Delta[CO_3^{2-}]$ in the upper 1000 m of the water column (Table 1, Fig. 6). Conversely, the slope of the Mg / Ca–water depth relationship becomes more gentle owing to the smaller change both in the BWT and $\Delta[CO_3^{2-}]$ with depth below 1000 m depth.

Although an exponential relationship between Mg / Ca and temperature is thermodynamically reasonable, some studies have reported that a linear fit is a more useful approximation (Toyofuku et al., 2000; Marchitto et al., 2007). Exponential and linear regressions of *C. wuellerstorfi* type B Mg / Ca on the BWTs that range from 1.7 to 16.3 °C yields the following relationships:

$$\mathrm{Mg/Ca} = 0.85\ (\pm 0.02)\exp(0.082\ (\pm 0.003)\ \mathrm{BWT}) \quad (1)$$
$$(R^2 = 0.97,\ P < 0.0001),$$

$$\mathrm{Mg/Ca} = 0.66\ (\pm 0.04) + 0.14\ (\pm 0.005)\ \mathrm{BWT} \quad (2)$$
$$(R^2 = 0.97,\ P < 0.0001),$$

where the standard errors of the coefficients and intercepts are given in parentheses. The standard deviation of the difference between the calculated and CTD temperature is ±1.1 °C for the exponential regression and ±0.92 °C for the linear regression. Based on these equations, the precision of replicate Mg / Ca analyses of ± 0.03 mmol mol^{-1} corresponds to ±0.2–0.3 °C, which is smaller than the standard deviation derived from the calibration data set. Our Mg / Ca data also show a strong positive correlation to $\Delta[CO_3^{2-}]$ ($R^2 = 0.95$) (Fig. 6c). Mg / Ca dependence on $\Delta[CO_3^{2-}]$ is 0.016 mmol mol^{-1} per µmol kg^{-1} and yields the following relationship:

$$\mathrm{Mg/Ca} = 0.016\ (\pm 0.0007)\ \Delta[CO_3^{2-}] + 0.93\ (\pm 0.04)$$
$$(R^2 = 0.95,\ p < 0.0001). \quad (3)$$

It is difficult to quantify the effects of BWT and $\Delta[CO_3^{2-}]$ in isolation owing to the robust relationship between them over this wide range of BWT (1.7 to 16.3 °C). Thus, we refer to the modern BWT vs. $\Delta[CO_3^{2-}]$ diagram to discuss in greater detail the effects of both BWT and $\Delta[CO_3^{2-}]$ on Mg / Ca (Fig. 6d). In the lower BWT range (i.e. less than ∼ 5 °C), modern $\Delta[CO_3^{2-}]$ is relatively constant (∼ 10 µmol kg^{-1}), allowing the effect of BWT to be evaluated. At these temperatures, the correlation is weaker but still statistically significant ($R^2 = 0.53$, $p < 0.0001$, Fig. 6e), yielding the following equation:

$$\mathrm{Mg/Ca} = 0.10\ (\pm 0.02)\ \mathrm{BWT} + 0.79\ (\pm 0.07)$$
$$(R^2 = 0.53,\ p < 0.0001). \quad (4)$$

The standard deviation of the difference between the calculated and CTD temperature is ± 0.96 °C (1σ). The slope of this relationship is more gradual than that in the wide BWT range, suggesting that the carbonate ion acts to amplify BWT sensitivity owing to the positive relationship between BWT and $\Delta[CO_3^{2-}]$. $\Delta[CO_3^{2-}]$ sensitivity at BWTs below ∼ 5 °C, where previous studies have reported higher $\Delta[CO_3^{2-}]$ sensitivity (< 25 µmol kg^{-1}) (Elderfield et al., 2006; Yu and Elderfield, 2008), could not be evaluated in our study, because the variation range of the modern $\Delta[CO_3^{2-}]$ is narrow at these BWTs (Fig. 6f). Although the sensitivity of 0.10 mmol mol^{-1} per °C is slightly higher than that for *C. wuellerstorfi* with the $\Delta[CO_3^{2-}]$ correction of Yu and Elderfield (2008) (0.03–0.07 mmol mol^{-1} per °C), it is close to the sensitivity for *Uvigerina* spp. in the Pacific (0.10 mmol mol^{-1} per °C), which is little affected by bottom water carbonate saturation because of its infaunal habitat (Elderfield et al., 2012).

For comparison with previous calibrations, all of the published Mg / Ca data for *C. wuellerstorfi* are plotted (Fig. 7a). Many of the data were obtained from the Atlantic but were limited in terms of their temperature range (i.e. less than ∼ 6 °C), with fewer data from the Pacific and other ocean basins (Table 3). The temperature range was extended to 8.7 °C in the Pacific using a data set from Rathburn and De Decker (1997), in which neither oxidative nor reductive cleaning steps had been conducted. Most of the published Mg / Ca data are scattered primarily around one linear line (∼ 0.3 mmol mol^{-1} per °C), except for those from the Norwegian Sea, which has very low BWT and high bottom water $\Delta[CO_3^{2-}]$ (Yu and Elderfield, 2008). Our Mg / Ca data deviate from previous data at higher temperatures (i.e. greater than ∼ 4–5 °C), and typically exhibit lower values than the data from both the Atlantic and Pacific.

Differences in cleaning procedure must be considered, because incorporation of a cleaning step without oxidative or reductive steps sometimes increases Mg / Ca values by more than ∼ 1 mmol mol^{-1} (Barker et al., 2003). The Pacific Mg / Ca data from Rathburn and De Decker (1997) were produced with a cleaning step without oxidative or reductive steps, and those from Martin et al. (2002), which were originally from Rosenthal et al. (1997), were cleaned with both steps. Nevertheless, Rathburn and De Decker's data appear to follow a linear fitting line and agree with the data of Martin et al. (2002); thus, these values do not appear to have been increased by the different cleaning procedure. In addition, the difference in obtained Mg / Ca between the oxidative and reductive methods is relatively small (∼ 0.09 mmol mol^{-1}) (Yu and Elderfield, 2008). Therefore, the lowest sensitivity of Mg / Ca to temperature does not appear to be caused by differences in cleaning protocols. This sensitivity difference can be attributed in part, but not wholly, to the carbonate ion effect, as discussed below. At 1200 m depth, the total alkalinity (TA) and DIC exhibit substantial south–north gradients in the Pacific (Key et al., 2004). The 1200 m DIC gradients are greater than those for TA, reflecting lower $[CO_3^{2-}]$ ($\Delta[CO_3^{2-}]$) in the high- and mid-latitude North Pacific than in the equatorial and South Pacific ($[CO_3^{2-}] \sim$ TA–DIC). The higher Mg / Ca in the Coral Sea (Rathburn and De Decker, 1997) and Ontong Java Plateau (Martin et al., 2002) may be explained partly by their higher $\Delta[CO_3^{2-}]$ than those in the western subtropical North Pacific.

To investigate the relationship between Mg / Ca and $\Delta[CO_3^{2-}]$ in greater detail, our Mg / Ca data together with previously published data are plotted in Fig. 7b. Four previous studies have presented $\Delta[CO_3^{2-}]$ values together with their Mg / Ca values (Elderfield et al., 2006; Yu and Elderfield, 2008; Raitzsch et al., 2008; Tisserand et al., 2013). Of these, the Mg / Ca values from Tisserand et al. (2013) appear

Table 3. Published Mg / Ca data from various oceans. Reduction: cleaning protocol including reductive and oxidative steps. Oxidation: cleaning protocol including only oxidative step. Leaching: only sonication and leaching were conducted. Sonication: only sonication was conducted.

Species	References	Ocean	Number of data	Cleaning/measurement method	Temperature range (°C)	$\Delta[CO_3^{2-}]$ range ($\mu mol\,kg^{-1}$)	Remarks
C. wuellerstorfi (*P. wuellerstorfi*)	Russell et al. (1994)	Atlantic, Pacific	11, 4	Reduction	1.7–2.8	–	
	Rosenthal et al. (1997)	Atlantic	3	Leaching	2.3–2.5	–	
	Rathburn and De Decker (1997)	Pacific	45	Sonication	2.7–8.7	–	
	Billups and Schrag (2002)	Pacific	1	Oxidation	1.6	–	
	Lear et al. (2002)	Atlantic, Pacific	6,10	Reduction	1.8–4.3	–	
	Martin et al. (2002)	Atlantic, Pacific	26, 13	Reduction	−1.1–3	–	Unpublished data by Rothernthal et al. are included.
	Healey et al. (2008)	Atlantic, Indian Ocean, South China Sea	22, 7, 4	Reduction	0.8–3.8	–	
	Raitzsch et al. (2008)	Atlantic	44	Laser ablation measurement	0.4–3.7	92–128	
	Yu and Elderfield (2008) including Elderfield et al. (2006)	Atlantic, Indian Ocean, Norwegian Sea, Pacific	94, 10, 28, 23	Oxidation/reduction	−1.1–4.4	−23–61	
	Tisserand et al. (2013)	Atlantic	34	Oxidation	4.1–6.6	33-38	
C. wuellerstorfi (*P. wuellerstorfi*) type B	This study	Pacific	28	Reduction	1.7–16.3	7–125	
C. pachyderma (*C. floridanus*)	Rathburn and De Decker (1997)	Pacific	2	Sonication	3.0–4.0	–	
	Rosenthal et al. (1997)	Atlantic	20	Leaching	4.5–18.4	–	
	Lear et al. (2002)	Atlantic, Pacific	13, 4	Reduction	2.4–18.4	–	
	Marchitto et al. (2007)	Atlantic	29	Reduction	5.8–18.6	46–161	

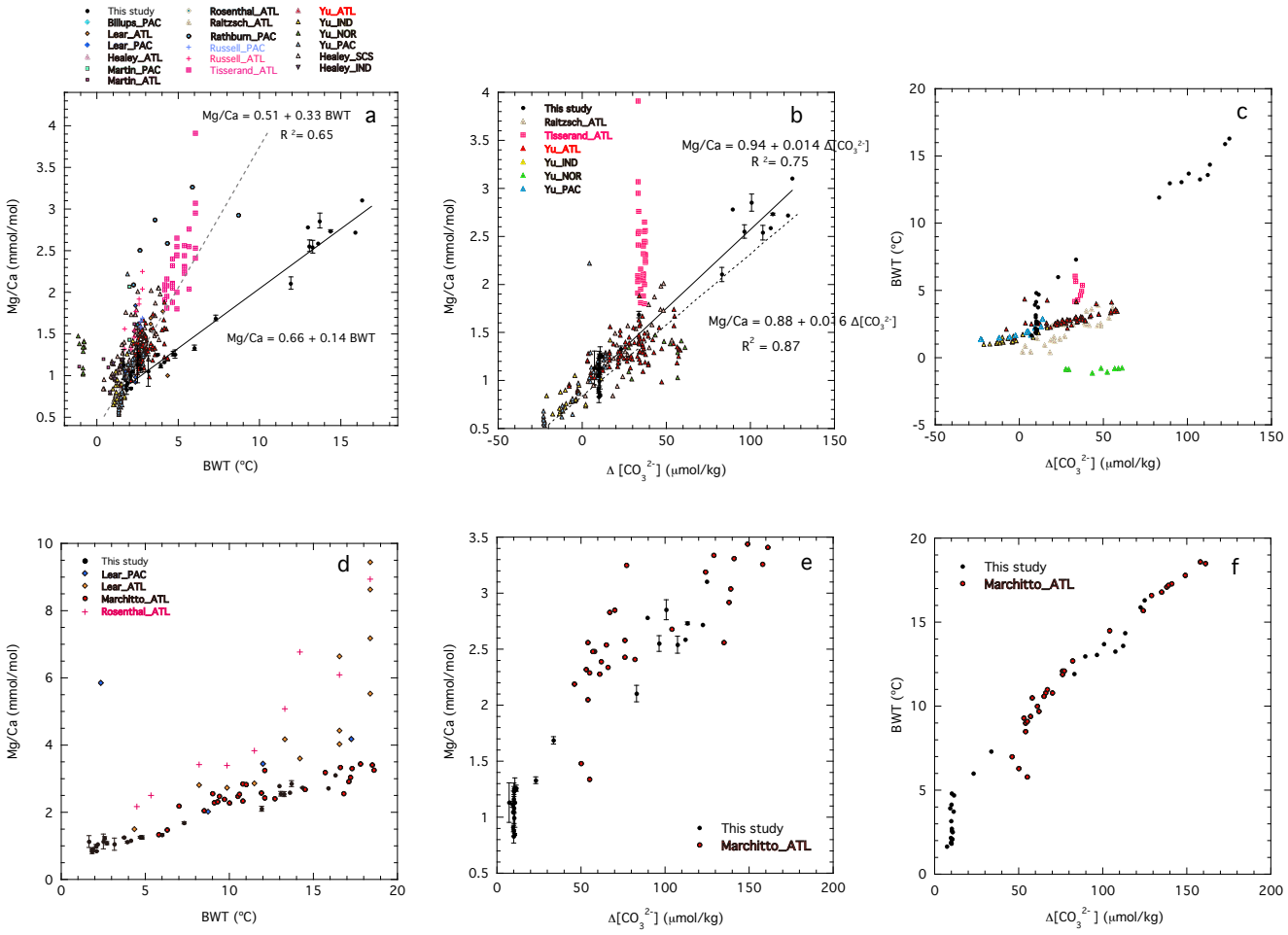

Figure 7. Comparison to previous Mg / Ca data. Mg / Ca values of *C. wuellerstorfi* including type B vs. (a) BWT and (b) $[\Delta CO_3^{2-}]$. (c) and (f) BWT vs. $[\Delta CO_3^{2-}]$ in the different ocean basins. Mg / Ca values of *C. wuellerstorfi* type B and *C. pachyderma* vs. (d) BWT and (e) $[\Delta CO_3^{2-}]$. All the data presented here are listed in Table 3. ATL: Atlantic, PAC: Pacific, IND: Indian Ocean, NOR: Norwegian Sea, SCS: South China Sea.

to deviate from the other data. Excluding data from Tisserand et al. (2013), there is a positive correlation ($R^2 = 0.75$) between BWT and $\Delta[CO_3^{2-}]$ over a wide range (Eq. 5).

$$\mathrm{Mg/Ca} = 0.014\ (\pm 0.0005)\ \Delta[CO_3^{2-}] + 0.94\ (\pm 0.018)$$
$$(R^2 = 0.75,\ p < 0.0001) \quad (5)$$

The sensitivity of Mg / Ca to $\Delta[CO_3^{2-}]$ of our study (0.014–0.016 mmol mol^{-1} per µmol kg^{-1}) is considerably higher than the 0.0083–0.010 mmol mol^{-1} per µmol kg^{-1} reported by previous studies (Elderfield et al., 2006; Healey et al., 2008; Raitzsch et al., 2008; Yu and Elderfield, 2008). This might be due to a steeper temperature rise vs. $\Delta[CO_3^{2-}]$ in the subtropical northwestern Pacific than in other regions (Fig. 7c).

Yu and Elderfield (2008) concluded that considering $\Delta[CO_3^{2-}]$ provided a satisfactory explanation for differences in the absolute Mg / Ca values of *C. wuellerstorfi* among different oceanic basins. In their study, the Mg / Ca sensitivity to temperature decreases to 0.03–0.07 mmol mol^{-1} per °C when the $\Delta[CO_3^{2-}]$ effect is taken into account. In contrast, Tisserand et al. (2013) demonstrated a very high Mg / Ca dependence on temperature (19 % increase per °C), even when the $\Delta[CO_3^{2-}]$ effect may be negligible (Fig. 7a, c). That is, the slope of Mg / Ca to temperature could change depending on $\Delta[CO_3^{2-}]$, even among same species. As mentioned by Marchitto et al. (2007), benthic foraminifera tend to incorporate less Mg / Ca when calcifying in both undersaturated and very supersaturated conditions. For the undersaturated condition, Yu and Elderfield (2008) suggested the possible existence of a $\Delta[CO_3^{2-}]$ threshold for changes in *C. wuellerstorfi* Mg / Ca at 25 µmol kg^{-1}: when $\Delta[CO_3^{2-}]$ is < 25 µmol kg^{-1}, *C. wuellerstorfi* Mg / Ca seems to be less sensitive to temperature changes. However, the Mg / Ca dependence in the supersaturated condition cannot be evaluated due to the lack of a larger data set extending into supersaturated waters for

C. wuellerstorfi. In addition, we cannot exclude the possibility that differences in *C. wuellerstorfi* types might affect Mg / Ca dependence through physiological differences.

It is interesting to provide a comparison between our Mg / Ca of *C. wuellerstorfi* type B and that of *C. pachyderma*. Among *Cibicidoides* species, Mg / Ca of *C. pachyderma* in the Florida Strait from Marchitto et al. (2007) fits well with our Mg / Ca of *C. wuellerstorfi* type B in Mg / Ca–BWT plots (Fig. 7d). The Mg / Ca data of Marchitto et al. (2007) are also in good agreement with our Mg / Ca data in the corresponding Mg / Ca-$\Delta[CO_3^{2-}]$ plot but more scattered (Fig. 7e). An overlapping variation pattern of BWT vs. $\Delta[CO_3^{2-}]$ could lead to the similarity in Mg / Ca values between *C. wuellerstorfi* B and *C. pachyderma* (Fig. 7f). Alternatively, one might argue that the similarity results from their common habitat or physiological characteristics. For example, Raitzsch et al. (2008) argued that interspecies differences in microhabitat might explain Mg / Ca differences. Typical *C. wuellerstorfi* prefers an elevated position above the sediment–water interface (Lutze and Thiel, 1989), while *C. pachyderma*, similar to *C. mundulus*, lives at deeper depths but within the sediment–water interface (Rathburn and Corliss, 1994). Although our knowledge of the ecology of *C. wuellerstorfi* type B remains very poor, *C. wuellerstorfi* type B might be less affected by the water carbonate saturation state of the bottom water than typical *C. wuellerstorfi* if it lives at deeper depths than typical *C. wuellerstorfi*.

6 Downcore results

6.1 Benthic Mg / Ca

The Mg / Ca values for GH08-2004 vary between 0.61 and 1.36 mmol mol^{-1} for the last 26 kyr (Fig. 8a). Mg / Ca was relatively high at 25 kyr BP, possibly coinciding with Heinrich event 2 (H2). Mg / Ca exhibits values of 0.83 mmol mol^{-1}, on average, during the LGM (18–22 kyr BP). For the last deglaciation, the Mg / Ca record exhibits a high peak at 17 kyr BP, likely coinciding with H1. Mg / Ca began to decrease by $\sim$ 0.3 mmol mol^{-1} from 17 to 14 kyr BP, and subsequently increased by $\sim$ 0.5 mmol mol^{-1} toward 11.5 kyr BP. Another high peak at 11.5 kyr BP seems to coincide with YD, although only a single data point supports the peak. Holocene Mg / Ca appears highly variable, ranging between $\sim$ 0.8 and $\sim$ 1.2 mmol mol^{-1} at the multi-millennial scale, with high peaks at 10.5, 8.2, and 5.3–5.6 kyr BP and low peaks at 9.6, 6.5, and 2.3 kyr BP.

6.1.1 Evaluation of carbonate saturation effect on Mg / Ca

It seems that the carbonate saturation state has not remained constant since the last glacial period (Yu et al., 2014). Although the core site is located well above the carbonate lysocline depth ($\sim$ 3500 m in the western tropical Pacific; Broecker and Peng, 1982), the potential effect of $\Delta[CO_3^{2-}]$ should be evaluated when interpreting the downcore Mg / Ca record. In order to estimate the carbonate ion effect on the temporal Mg / Ca changes, we present another proxy, an index using *G. menardii* fragmentation, which can reflect the carbonate saturation state; however, this is a qualitative measure. Tests of the planktic foraminifera *G. menardii* are sensitive to carbonate dissolution, and attrition of *G. menardii* tests correlates well with the fraction of calcite dissolved (Ku and Oba, 1978; Mekik et al., 2002). All specimens of *G. menardii* were picked from an assemblage sample, and the numbers of the following specimens were counted: (a) undamaged specimens; (b) almost whole specimens, or those with more than half of the original specimen remaining; (c) specimens with less than half remaining; and (d) fragments of keels only (Mekik et al., 2002). Then, the *G. menardii* fragmentation index (MFI: Mekik et al., 2002) was calculated according to the following equation of Mekik et al. (2002):

$$\mathrm{MFI} = (b + (c/3) + d/5)/(a + b + (c/3) + d/5). \quad (6)$$

The MFI record of GH08-2004 is exhibited together with the percentage of perfect tests (Fig. 8b), indicating generally better carbonate preservation during glacial times than during the Holocene. This may be related to the higher carbonate saturation state at water depths less than $\sim$ 2 km during glacial time, possibly due to lower atmospheric CO_2 concentrations (e.g. Bertram et al., 1995). During the last deglaciation, the temporal variation in carbonate preservation state does not correlate with Mg / Ca (Fig. 8). There is no correlation between the benthic Mg / Ca and % dissolution ($R = 0.052$, $p = 0.754$), suggesting that carbonate saturation state is unlikely to affect Mg / Ca.

For planktic foraminiferal Mg / Ca, post-depositional carbonate dissolution decreases Mg / Ca at low saturation level (bottom water $\Delta[CO_3^{2-}] < 30$ µmol kg^{-1}) (Regenberg et al., 2014). However, this is the case for planktic foraminifers but not benthic foraminifers; that is, the post-depositional dissolution effect on Mg / Ca is negligible for benthic foraminifers (Lear et al., 2002; Elderfield et al., 2006).

6.1.2 Conversion of foraminiferal Mg / Ca to temperature

As described in Sect. 5, we report the Mg / Ca–BWT conversion equations depending on the two temperature ranges. Eqs. (1) and (2) contain the effect of the carbonate ion component, while this component can be negligible in Eq. (4).

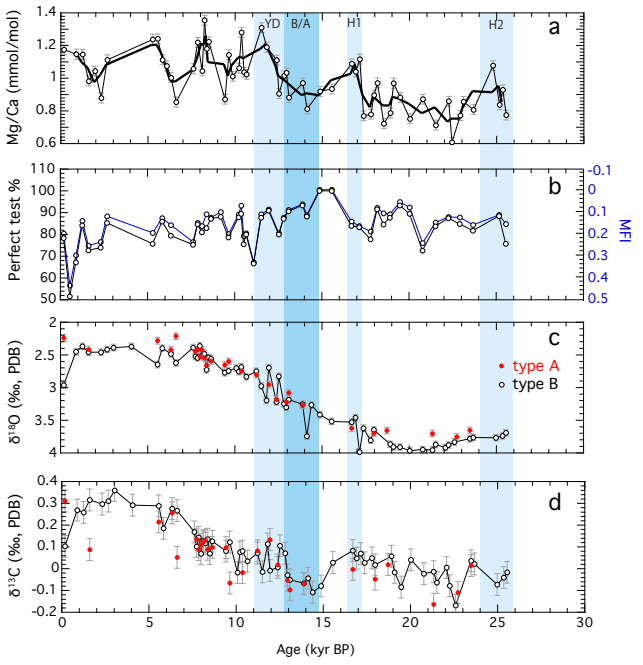

Figure 8. **(a)** Mg / Ca, **(b)** perfect test % (in black) and MFI (in blue), **(c)** $\delta^{18}O_c$ (original values), and **(d)** $\delta^{13}C_c$ (original values) vs. calendar age for GH08-2004. **(c, d)** Filled red circles represent $\delta^{18}O_c$ and $\delta^{13}C_c$ data from *C. wuellerstorfi* type A, and open circles represent *C. wuellerstorfi* type B. H1, B/A, and YD represent Heinrich 1, Bølling–Allerød, and Younger Dryas intervals. The bold line in **(a)** indicates three-point running mean. Analytical errors are expressed as bars.

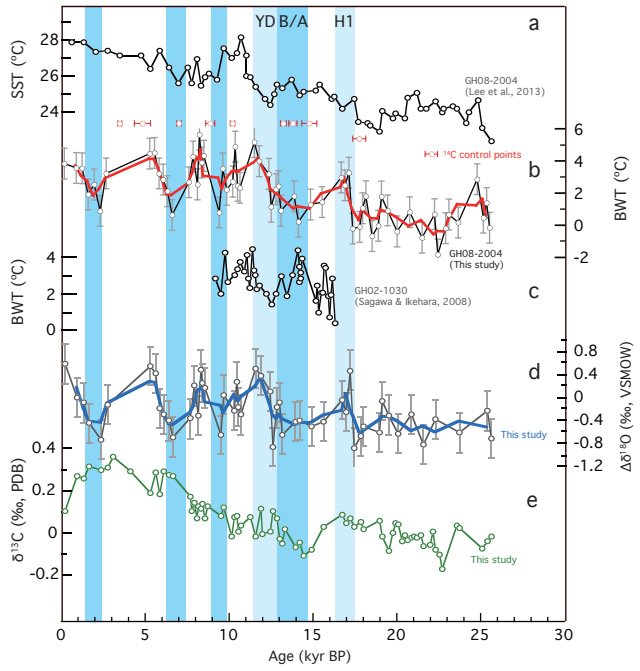

Figure 9. **(a)** Sea surface temperature (SST) derived from Mg / Ca of the planktic foraminifera *G. ruber* of core GH08-2004 (Lee et al., 2013), **(b)** bottom water temperature (BWT) of core GH08-2004 (this study), **(c)** Mg / Ca-derived BWT of *U. akitaensis* of core GH02-1030, 1212 m water depth in the subarctic western North Pacific (Sagawa and Ikehara, 2008), and **(d)** local $\delta^{18}O_w$ ($\Delta\delta^{18}O_w$) and **(e)** benthic $\delta^{13}C$ of GH08-2004 (this study). Bold lines indicate three-point running mean in **(b)** and **(d)**. The ± 1 °C errors and propagated errors are expressed as error bars in **(b)** and **(d)**.

Moreover, the modern BWT of the core site is 3.0 °C, which is within the range of Eq. (4), and most of the downcore Mg / Ca values were lower than the core-top value. Therefore, Eq. (4) can be regarded as more appropriate for conversion of the downcore Mg / Ca record. The Mg / Ca values of core GH08-2004 were converted to temperature by the linear fitting using Eq. (4), because little difference is seen between the linear fitting and exponential fitting (Fig. 6e).

6.1.3 BWT variation

Average BWT during the LGM was found to be 0.4 ± 1.0 °C; thus, BWT during the LGM was ~ 2.6 °C lower than today (Fig. 9b). Subsequently, BWT increased by 2.5–3 °C at 17 kyr BP, then exhibited a decreasing trend (by ~ 2 °C overall) toward B/A. BWT appears to have increased again at about 12.5 kyr BP during YD. During the Holocene, BWT was highly variable, with variability of ± 1.4 °C (1σ). The bottom water was warmer at 11.5, 8.2–8.4, and 5.3–5.6 kyr BP, and was cooler at ~ 9.3, ~ 6.5, and ~ 2.3 kyr BP.

6.2 Benthic δ^{18} O and conversion to local δ^{18}O of seawater

For a best estimate of oxygen isotopic equilibrium, adjustment is needed for some benthic species, and is estimated to be +0.64 ‰ for *C. wuellerstorfi* (Shackleton et al., 1984). The difference in $\delta^{18}O_c$ between *C. wuellerstorfi* type A and type B ($\delta^{18}O_{c\ (\mathrm{typeB-A})}$) is $+0.081 \pm 0.19$ (1σ) ‰ ($n = 25$), which is larger than the analytical error. Thus, we applied the adjustment factor of +0.56 ‰ ($= 0.64 - 0.081$) for *C. wuellerstorfi* type B.

The $\delta^{18}O_c$ from core GH08-2004 exhibits a glacial transition, and has gradually decreased from ~ 4.0 to ~ 2.5 ‰ from the LGM to the present (Fig. 8c). The 1.5 ‰ difference in $\delta^{18}O_c$ between the LGM and the present is 0.4–0.5 ‰ larger than that expected based on the global ice volume effect (Schrag et al., 2002). We used the palaeotemperature equation of Shackleton (1974) to compute variations in $\delta^{18}O$ of bottom water ($\delta^{18}O_w$). The $\delta^{18}O_w$ was obtained in the PDB scale and converted to the VSMOW scale as follows ($\delta^{18}O_w$ (VSMOW) $= \delta^{18}O_w$ (PDB) + 0.27 ‰; Hut, 1987):

$$T = 16.9 - 4.38\,(\delta^{18}O_c - \delta^{18}O_w) + 0.10\,(\delta^{18}O_c - \delta^{18}O_w)^2. \quad (7)$$

Subsequently, the ice volume offset (Waelbroeck et al., 2002) was subtracted from $\delta^{18}O_w$, yielding a local $\delta^{18}O_w$ ($\Delta\delta^{18}O_w$) (Fig. 9d). Eventually, ± 0.34 ‰ of $\Delta\delta^{18}O_w$ error is derived based on adding the error for the ice volume offset (± 0.1 ‰) to ± 0.24 ‰ (1σ), which is the propagated error of $\delta^{18}O_w$ from BWT reconstruction when a BWT error of ± 0.96 °C is applied (0.25 ‰ per 1 °C). A core top yields $\Delta\delta^{18}O_w$ of 0.57 ‰, which is ~ 0.9 ‰ higher than that expected in equilibrium with ambient water (-0.3 to -0.4 ‰, Suzuki et al., 2010). Even assuming a modern $\delta^{18}O_w$ value of -0.13 ± 0.03 ‰ (1σ, $n = 91$), which is an average value for 1000–2000 m water depth in the northwestern Pacific (120–180° E, 20–60° N; Schmidt et al., 1999), the difference is still large (~ 0.7 ‰). Considering that $\delta^{18}O_c$ of *C. wuellerstorfi* type B increases by ~ 0.5 ‰ in the youngest horizon (core top) and exhibits a large difference from the $\delta^{18}O_c$ value of *C. wuellerstorfi* type A, we prefer not to rely on the core-top value. Middle to late Holocene average $\Delta\delta^{18}O_w$, including the core top, is -0.09 ± 0.39 ‰(1σ, $n = 8$), which approaches the modern $\delta^{18}O_w$ value of ambient seawater. Average $\Delta\delta^{18}O_w$ during the LGM was -0.5 ± 0.1 ‰, which is 0.4 ‰ lower than the middle to late Holocene average. In general, $\Delta\delta^{18}O_w$ exhibits a negative correlation with BWT (Fig. 9). The variability of $\Delta\delta^{18}O_w$ is ± 0.41 ‰ (1σ) throughout the record. Compared to the Mg / Ca results, higher $\Delta\delta^{18}O_w$ intervals at 17, 11.5, 8.2–8.4, and 5.3–5.6 kyr BP basically coincided with warmer BWT peaks, while lower $\Delta\delta^{18}O_w$ intervals at 17.5, 12.5, 6.5, and 2.3 kyr BP coincided with cooler BWT peaks (Fig. 9).

6.3 δ^{13} C variations

The $\delta^{13}C$ of epifaunal benthic foraminifera living at the bottom water–surface sediment interface was used to estimate changes in water mass $\delta^{13}C_{DIC}$ composition, and *Cibicidoides* reflect $\delta^{13}C_{DIC}$ in ambient water with a defined genera- or species-dependent offset in $\delta^{13}C_c$ (Graham et al., 1981; McCorkle et al., 1990, 1997). The $\delta^{13}C_c$ offset is zero for *C. wuellerstorfi*, and the difference between type A and type B ($\Delta\delta^{13}C_{c\ (typeB-A)}$) is 0.03 ± 0.10 ‰ ($n = 25$). Although this is not significant compared to analytical error, an adjustment factor of -0.03 ‰ was applied for the $\delta^{13}C_c$ record of *C. wuellerstorfi* type B. The middle to late Holocene average $\delta^{13}C_c$ is 0.28 ‰ ($n = 8$), which is within the modern range of $\delta^{13}C_{DIC}$ at 1000–2000 m water depth at 0–20° N (-0.25 to $+0.25$ ‰, Bostock et al., 2010), when the analytical error is considered. Downcore benthic $\delta^{13}C_c$ exhibits lower values for the LGM section, with low peaks at 22.5 and 19.5 kyr BP (Fig. 8d). Average $\delta^{13}C_c$ during the LGM was ~ 0.29 ‰ lower than the middle to late Holocene average. A shift in $\delta^{13}C_c$ from 17 to 14.5 kyr BP was in accordance with the gradual decrease in BWT. The $\delta^{13}C_c$ then shifted to higher values at 13 kyr BP, coinciding with the beginning of YD. During the Holocene, $\delta^{13}C_c$ shifted by approximately 0.2 ‰ during the time interval from 8 to 7 kyr BP, and decreased from 3 kyr BP to present.

7 Discussion

7.1 The Last Glacial Maximum

During the last glacial period, a water mass corresponding to the modern NPIW is thought to have been thicker and to have penetrated more deeply into the North Pacific (Matsumoto et al., 2002). In contrast, recent studies reveal that the deep ocean at the LGM was poorly ventilated, based on older benthic ^{14}C ages (Rae et al., 2014). These deep waters were isolated from the atmosphere, accumulating DIC effectively (Sarnthein et al., 2013). Without a drop in the deep North Pacific pH, the increase in alkalinity acted to buffer such an increase in DIC storage (Rae et al., 2014). Our MFI record suggests the better preservation of $CaCO_3$ during the LGM, supporting the higher pH. The $\delta^{13}C_c$ record exhibits lower values during the LGM than at present, consistent with $\delta^{13}C$ distribution compiled by Schmittner (2012) for the LGM. The surface productivity might have increased during the LGM, as inferred by an increase in total organic carbon in GH08-2004 during this period (Amano and Itaki, 2015), and the subsequent increased remineralisation would have decreased $\delta^{13}C_c$.

The average $\delta^{18}O_w$ during the LGM (18–22 kyr BP) is ~ 0.5 ‰ lower than a previously reconstructed $\delta^{18}O_w$ value of deep water (3290 m) in the South Pacific (Adkins et al., 2002). The modern $\delta^{18}O_w$–salinity relationship at depths greater than 300 m is $\delta^{18}O_w = 0.42$ salinity -14.6 in the area between 120 and 180° E and 20 and 60° N in the North Pacific ($R^2 = 0.81$) (Fig. 10, data from Schmidt et al., 1999). A modern deep water value of salinity and $\delta^{18}O_w$ in the South Pacific (Adkins et al., 2002) plots near an end member in the $\delta^{18}O_w$–salinity diagram of the Fig. 10, indicating a quite homogeneous distribution of $\delta^{18}O_w$ in the modern deep Pacific. This is also indicative of the simple mixing between higher salinity (higher $\delta^{18}O_w$) water from the south and lower salinity (lower $\delta^{18}O_w$) of NPIW in the North Pacific. The LGM intermediate $\delta^{18}O_w$ in the northwestern Pacific was much lower than that in the South Pacific. The difference in $\delta^{18}O_w$ between intermediate northwestern Pacific and South Pacific during the LGM was ~ 0.4 ‰, much larger than at present (less than 0.1 ‰). Exceeding the propagated error range of $\delta^{18}O_w$ reconstruction, the increase in this $\delta^{18}O_w$ difference during the LGM seems probable. Given that the $\delta^{18}O_w$–salinity relationship during the LGM was likely similar to today, as suggested by a coupled climate model (Roche et al., 2004), the salinity difference between the two regions was greater during the LGM than at present. Applying the modern slope of $\delta^{18}O_w$ to salinity (2002) yields 35.17 ± 0.57 for the LGM bottom water salinity at site GH08-2004. According to Adkins et al. (2002), by calculating a salt mass balance, the mean Pacific salinity was estimated to be 35.90 during

the LGM. However, this value is too low compared with the reconstructed deep water salinity of 36.19 in the South Pacific, implying the existence of a mass of low-salinity water in the North Pacific (Adkins et al., 2002). Our study provides evidence to support this implication. As for the Pacific density distribution during the LGM, the temperature gradient between the intermediate North Pacific and the deep South Pacific (Adkins et al., 2002) was similar to current values, but the salinity gradient was greater (∼ 1 in salinity) than at present (∼ 0.2–0.3 in salinity). Therefore, the intermediate–deep vertical density gradient was greater in the Pacific during the LGM than at present. This density structure would lead to stratification, suppressing the mixing between deep and intermediate waters in the Pacific. The stratified ocean would be favourable carbon storage in the deep Pacific.

7.2 The last deglaciation

During H1, the greater production and the deeper penetration of NPIW were suggested by the modelling study of Okazaki et al. (2010). The main source area of NPIW likely shifted to the Bering Sea from the Okhotsk Sea (Ohkushi et al., 2003; Horikawa et al., 2010; Rella et al., 2012) and spread south to the California margin in the eastern North Pacific (e.g. Keigwin and Jones, 1990; Behl and Kennett, 1996; Tada et al., 2000; Hendy and Pedersen, 2005). Although Jaccard and Galbraith (2013) argued that the well-ventilated waters penetrated to at most 1400–2400 m depth during H1, recent benthic and planktic ^{14}C data provide evidence that the deep North Pacific, at least 3400 m water depth, was well ventilated from 17.3 to 16 kyr BP (Rea et al., 2014). Despite the data discrepancy regarding the penetration depth, there is a common view that at least the upper 1400 m of water was filled by well-ventilated NPIW in the subarctic North Pacific during H1, trigged by an increase in surface density, which resulted from salinity increase promoted by a positive-salinity feedback (Okazaki et al., 2010).

The bottom water warming at 17 kyr BP in GH08-2004 seems to coincide with the time at which well-ventilated NPIW started to fill the intermediate depths in the subarctic North Pacific. Recent modelling results based on both an earth model of intermediate complexity, LOVECLIM, and a coupled general circulation model, MIROC, simulated intermediate (∼ 300–1200 m) warming in the Pacific Basin between ∼ 30° N and ∼ 30° S as a result of reduced upwelling of cooler water from the abyssal Pacific, related to a decrease in the return flow of PDW during H1 (Chikamoto et al., 2012). The bottom water warming at 17 kyr BP could be explained by a lesser contribution of PDW and greater contribution of NPIW in the subtropical northwestern Pacific.

At present, the bottom water of the site is influenced both by NPIW, which intrudes directly from the northeastern side of the basin (∼ 20–26° N), and by the waters flowing from the southeastern edge of the basin (∼ 9–15° N). Because the waters from the southeastern side enter at deeper depth

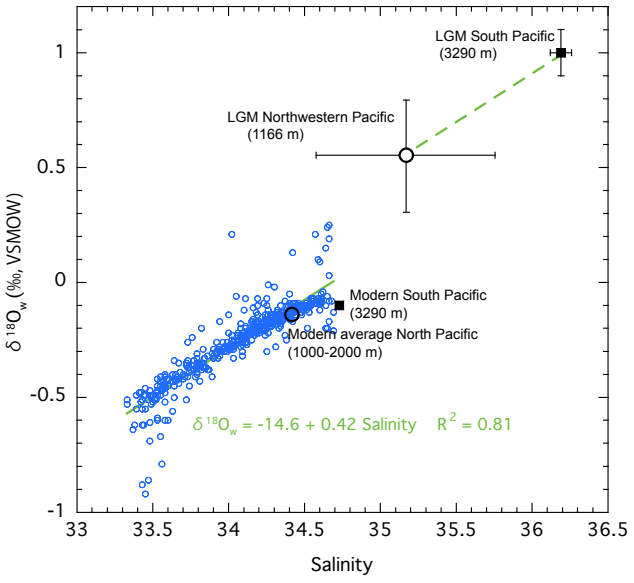

Figure 10. The modern $\delta^{18}O_w$–salinity relationship at depths greater than 300 m is $\delta^{18}O_w = 0.42$ salinity-14.6 in the area between 120 and 180° E and 20 and 60° N in the North Pacific (data from Schmidt et al., 1999). The deep water (3290 m water depth) values of salinity and $\delta^{18}O_w$ at present and at the LGM in the South Pacific (Adkins et al., 2002) are represented by black squares. The open circles represent the modern average value in the North Pacific (1000–2000 m water depth) and the estimated LGM of the study site in the northwestern Pacific.

(∼ 1500 m), today these waters are mainly from PDW, with a minor contribution of NPIW (Kaneko et al., 2001). In the case of 17 kyr BP, it seems feasible that the contribution of PDW at site GH08-2004 decreased through reduced inflow from the southeastern edge of the basin, and NPIW inflow along the northeastern edge increased. The greater production of NPIW might suppress upwelling of PDW; as a consequence, depths at which the PDW returned southward would shift to deeper depths (Matsumoto et al., 2002; Jaccard and Galbraith, 2013).

However, these changes in waters are not clear in our $\delta^{13}C_c$ record, which shows little change between the LGM and H1. Local primary productivity does not seem to explain the lack of the change in $\delta^{13}C_c$, because primary productivity at this site seems to be suppressed, based on the reduced carbon mass accumulation rate (Amano and Itaki, 2015).

At 17 kyr BP, it was necessary for more heat and saline water to be transported to the high latitudes in the North Pacific to form more dense waters (Okazaki et al., 2010). A planktic foraminiferal Mg / Ca record shows ∼ 1 °C rise in SST in the same core during H1 (Lee et al., 2013), which appears to coincide with BWT increase. The increase in the benthic $\Delta\delta^{18}O_w$ in association with the bottom water warming at 17 kyr BP in core GH08-2004 is consistent with decrease in precipitation in the North Pacific in response to reduced moisture transport from the equatorial Atlantic as a re-

sult of the AMOC collapse (Okazaki et al., 2010; Chikamoto et al., 2012). The intensified PMOC would have acted as a positive feedback in accordance with the Stommel feedback scenario (Stommel, 1961), as this intensified PMOC supplied the subtropical saline water to the high latitudes (Okazaki et al., 2010; Chikamoto et al., 2012). The intensified subtropical gyre, in accordance with the intensified subarctic gyre, could enhance the Kuroshio, leading to greater heat and salt transport to the high latitudes.

Following H1, BWT tended to decrease, in contrast to the continued rise of SST toward B/A (Lee et al., 2013). Another BWT record based on Mg / Ca of *Uvigerina akitaensis* from core GH02-1030 off northern Japan (42° 13.77′N, 144° 12.53′E; 1212 m water depth) exhibits a pattern opposite to our record, with warming at the beginning of B/A and subsequent cooling during YD (Sagawa and Ikehara, 2008; Fig. 9c). This discrepancy is unlikely due to the uncertainty in the age models, because the age differences in the temperature peaks between the two cores were much larger than the errors expected based on ^{14}C measurements. Because the two core sites are situated in different oceanic basins, the bottom water of GH02-1030 is likely influenced directly by NPIW, while the proportion of NPIW decreases as the main inflow of intermediate/deep water enters from the southeastern edge in the Philippine Basin, lessening the influence of NPIW. That is, the BWTs of GH02-1030 may reflect water properties close to the end member of NPIW, whereas those of GH08-2004 reflect a mixture of PDW and NPIW and, therefore, changes in their mixing ratios. The BWT of GH02-1030 was 3–4 °C during B/A, whereas our record shows 0–2 °C. This might be interpreted as the greater influence of PDW (which has a colder temperature) at our site than at GH02-1030, or could simply be the result of poor temporal resolution in our BWT record, because the warm interval during B/A in GH02-1030 is short (less than 1 kyr) and only three data points cover this interval in our record. Decreasing BWT toward B/A in our record is not the consequence of direct influence of NPIW; rather, it reflects temporal changes in mixing ratio to the higher contribution of PDW, which was likely induced by enhancement of the upwelling of the abyssal water and subsequent increased return flow of PDW in the North Pacific Basin. Accordingly, the depths of lowest $\delta^{13}C_{DIC}$ were possibly shallow, and $\delta^{13}C_{DIC}$ of the intermediate depths in the North Pacific became more depleted. The decline in $\delta^{13}C_c$ in association with decrease in the BWT is consistent with this view. A uranium record at 682 m water depth, obtained by Jaccard and Galbraith (2013), indicates depleted oxygen in the North Pacific and supports the assertion that intermediate depths in the Pacific experienced greater contributions of PDW during the B/A than today.

The BWT in GH08-2004 appears to have started to increase again at 12.5 kyr BP, reaching its warmest temperature at 11.5 kyr BP during YD, although the temporal resolution during this interval is poor. At the beginning of YD, $\delta^{13}C_c$ of GH08-2004 also increased. Although the pattern of the benthic $\delta^{13}C_c$ did not match perfectly with that of BWT during YD, both records imply a temporal reduction in deep water upwelling during YD and/or a deeper penetration of NPIW similar to that of H1. The increased production rate of NPIW possibly resulted from an increase in salinity, inferred from the increase in $\delta^{18}O_w$.

7.3 The Holocene

At present, variations in ocean circulation during the Holocene remain poorly understood in the Pacific Ocean. Our data demonstrate that the Holocene variability of BWT and $\delta^{18}O_w$ in the subtropical northwestern Pacific is large at millennial to multi-millennial timescales, despite the more stable climate conditions. The amplitude of BWT variation is surprisingly large during the Holocene and is the same as that during the deglaciation, suggesting that the Holocene circulation shift is drastic. The variations in BWT probably reflect the shift in intermediate and deep water circulation in the North Pacific, which are likely explained by the changes in the mixing ratio between PDW and NPIW.

At present, NPIW is formed through brine rejection and the sinking of dense shelf waters in the Okhotsk Sea, which is tightly coupled to winter northerly winds over the Okhotsk Sea (e.g. Kitani, 1973; Talley, 1991). Cold northerly winds over the Okhotsk Sea are associated with the strengthened Aleutian Low over the Okhotsk Sea, which is expressed as negative mode of the Arctic Oscillation (AO), while the positive mode of the AO is associated with warmer autumn SST and reduced winter sea ice in the Okhotsk Sea (Ogi and Tachibana, 2006). A recently published high-resolution alkenone-derived SST shows higher SST peaks at ∼ 10.5, ∼ 9, and 7–6 kyr BP in the southern Okhotsk Sea (LV29-114-3; Max et al., 2012). The alkenone record is interpreted as reflecting the late summer/autumn surface temperatures, based on modern alkenone production, thus could be closely coupled to the strength of the Aleutian Low and hence NPIW production. Three other alkenone records from the southern Okhotsk Sea also show higher SSTs at 10.5–9 and 7–6 kyr BP (XP98-PC-2 and -PC-4; Seki et al., 2004, and MD01-2412 in Harada et al., 2006). The higher SSTs at 3–2 kyr BP are weakly distinguishable in lower-temporal-resolution alkenone records from the southern Okhotsk Sea (Seki et al., 2004; Harada et al., 2006), except for in core LV29-114-3 (Max et al., 2012). The weakening of the Aleutian Low and the lessening of the NPIW production are inferred from this surface water warming in the Okhotsk Sea during these time intervals. The cooling of bottom water in the subtropical northwestern Pacific at ∼ 10.5–9, 7–6 kyr BP, and 3–2 kyr BP coincides with these warmer surface waters in the Okhotsk Sea, which are in line with less NPIW contribution and greater contribution of the cooler PDW. Conversely, the bottom water warming in the subtropical northwestern Pacific could be caused by the reduction of the PDW upwelling owing to the greater production of the NPIW. The

bottom water warming at 8 kyr BP in the subtropical northwestern Pacific coincided with the cooling in the Okhotsk Sea (Max et al., 2012). Although the temporal resolution of our data is low during the middle Holocene, the bottom water in the subtropical northwestern Pacific tended to be warmer at ∼ 5 kyr BP, correlating with a pronounced SST minimum at 6–3 kyr BP in the Okhotsk Sea (Seki et al., 2004; Harada et al., 2006; Max et al., 2012). Although there is some regional difference in terms of the secular SST trend from the middle to the late Holocene in the Okhotsk Sea, as discussed by Max et al. (2012), the millennial- to multi-millennial-scale variations are generally consistent with the interpretation of the NPIW production rate, inferred from our BWT record.

The benthic and planktic ^{14}C data from the northern South China Sea, close to our study site, provide evidence for age variations of the intermediate water, although the temporal resolution is low (Wan and Jian, 2014), supporting our interpretation. The ages of the intermediate water in the northern South China Sea were remarkably younger during 5–3 kyr BP, suggesting the influence well-ventilated water, most likely NPIW. Conversely, the intermediate water in the northern South China Sea tended to be older at 9, 7, and 2 kyr BP, despite the lower temporal resolution of Wan and Jian (2014), suggesting the greater contribution of the older PDW. However, our BWT and the alkenone–SST records from the southern Okhotsk Sea are inconsistent with a projection age record based on time-series benthic ^{14}C data of C9002A from off Shimokita peninsula in northern Japan (41°11′01.20″N, 142°12′01.97″E; 1179 m water depth), which marks a relatively older projection age at ∼ 10.5–9 and 3–2 kyr BP but younger projection age at 7–6 kyr BP (Rella and Uchida, 2014). A possible explanation for the discrepancy for 7–6 kyr BP is changes in the source of the waters in the Okhotsk Sea, i.e. the reservoir age of the waters in the Okhotsk Sea was much younger at 7–6 kyr BP.

The variations in $\delta^{18}O_w$ cannot simply be explained by the changes in the mixing ratio between PDW and NPIW if the modern $\delta^{18}O_w$ values of PDW and NPIW are applied. As the salinity of the NPIW is lower than that of PDW, the $\delta^{18}O_w$ of NPIW is accordingly lower than that of PDW. Assuming this relationship throughout the entire Holocene, the $\delta^{18}O_w$ data are inconsistent with the interpretation based on the BWT record. Given the consistency of our BWT data and SST in the Okhotsk Sea, BWTs are considered more likely to capture the circulation change signals. Therefore, the $\delta^{18}O_w$ variations are interpreted as changes in source water $\delta^{18}O_w$ instead of changes in the mixing ratio between NPIW and PDW. When salinity increases at the surface, reduced precipitation or increased evaporation act to increase $\delta^{18}O_w$; conversely, increases in sea ice formation, which most likely occur in the subarctic area, have little effect on $\delta^{18}O_w$ (O'Neil, 1968). For example, $\delta^{18}O_w$ would decrease by only 0.1 ‰ for a salinity increase of 2, assuming that fractionation between water and ice ($\Delta\delta^{18}O_{ice-water}$) is 0.2 ‰ (Sharp, 2007). The large amplitude in the $\delta^{18}O_w$ variations implies that salinity increase or decrease is caused by the precipitation–evaporation balance rather than changes in sea ice formation. If the modern $\delta^{18}O_w$–salinity relationship is applied, 0.4 ‰ variability in $\delta^{18}O_w$ is equivalent to 1 in salinity. The increase in $\delta^{18}O_w$ (salinity), which likely correlates with the higher production rate of NPIW, suggests that the more saline water in the source region is favourable to the formation of dense water and promotes the production of NPIW.

8 Conclusions

Based on the 28 surface sediment samples around Okinawa Island, we reported Mg / Ca temperature-conversion equations for the temperature range of 1.7 to 16.3 °C for *C. wuellerstorfi* type B. Our Mg / Ca slope was lower than those in previous studies for *C. wuellerstorfi*, which cannot be simply explained by the difference in $\Delta[CO_3^{2-}]$ among various oceanic basins. This outcome is the result of complex influences of $\Delta[CO_3^{2-}]$ on Mg / Ca and/or differences in the microhabitat between the two types. Nevertheless, we found a significant correlation between Mg / Ca and BWT for type B at $\Delta[CO_3^{2-}]$ of approximately 10 µmol kg^{-1} (0.1 mmol mol^{-1} per °C), corresponding to BWT below 5 °C, and applied it to reconstruct BWT and bottom water $\Delta\delta^{18}O_w$ of core GH08-2004. Our results suggest that the greater vertical and north–south salinity (and probably density) gradient in the Pacific would lead to stratification, which would be favourable to carbon storage in the deep Pacific. The bottom water warming at 17 kyr BP is plausibly interpreted as a reduced supply of cooler abyssal water to the intermediate depths of the North Pacific and increased contribution of NPIW to our core site. After the intermediate warming, BWT decreased from 17 to 14.5 kyr BP, in association with the decrease in benthic $\delta^{13}C_c$, suggesting changes in relative contribution of NPIW (PDW) from higher (lower) to lower (higher). Another peak in BWT and $\delta^{18}O_w$ at 11.5 kyr BP (YD) suggests the greater production of NPIW, similar to H1. The bottom water variability seems to have been large during the Holocene, suggesting drastic ocean circulation changes under stable climate conditions.

Taxonomic note

Cibicidoides wuellerstorfi type B

Diagnostic

Test moderate to large, compressed planoconvex; approximately 10–12 chambers in the final whole increase rapidly in size, separated by slightly depressed, strongly curved sutures, hooked in final chambers on umbilical side; umbilical side low conical, granular in appearance, sutures incised; spiral side flat to slightly convex, coarsely perforated; aperture

small, peripheral, narrow-lipped but sometimes not distinctive, extends onto spiral side.

Description

Tests are thicker and more robust than typical *Cibicidoides wuellerstorfi* (Schwager) (i.e. *Planulina wuellerstorfi* or *Fontbotia wuellerstorfi*) (Holbourn et al., 2013). Except for the granular surface texture, there are no differences in morphology between both species. At this moment, it is considered reasonable and proper that this species is classified as *C. wuellerstorfi* (Schwager) from the morphological point of view. *C. wuellerstorfi* type B has common characteristics in terms of granular and more robust tests with *Planulina renzi* Cushman and Stainforth, but differs by its less flattered form, fewer chambers, and more depressed sutures. *C. wuellerstorfi* type B differs from *Cibicides dispars* (d'Orbigny), which is characterised by its more bloated umbilical side and flattened umbilicus.

Remarks

The ecology of *C. wuellerstorfi* type B is differentiated from that of the typical *C. wuellerstorfi* by its much shallower habitat. The habitat depth of the typical *C. wuellerstorfi* is thought to be primarily bathyal (Holbourn et al., 2013). In contrast, *C. wuellerstorfi* has been found at 400 m depth around New Zealand (Hayward et al., 2010). Thus, the habitat depth of this species may be different between localities, depending on environmental factors such as the level of food availability (Altenbach et al., 1999).

The Supplement related to this article is available online at doi:10.5194/cp-11-803-2015-supplement.

Acknowledgements. We sincerely thank the scientists and crew of cruises GH08, GH09, and GH10 of R/V *Hakurei-maru No. 2* for their sampling assistance. We also thank S. Hasegawa and H. Uchimura for identification of the benthic foraminifera. The analyses were supported by staff at the MIO, JAMSTEC, including H. Yamamoto, T. Omura, and N. Kisen. This study was funded by the Japan Society for the Promotion of Science (JSPS) Kakenhi, grant numbers 21740373, 25400504, 23221022, and 26247085. This study was funded by a grant-in-aid for JSPS Fellows, grant number 10914, awarded to Y. Kubota. This research was also supported by a grant from the Japan Agency for Marine-Earth Science and Technology (JAMSTEC) from the Ministry of Education, Culture, Sports, Science, and Technology (MEXT, Japan).

Edited by: M. Mohtadi

References

Adkins, J. F., McIntyre, K., and Schrag, D. P.: The salinity, temperature, and $\delta^{18}O$ of the glacial deep ocean, Science, 298, 1769–1773, 2002.

Ahagon, N., Ohkushi, K., Uchida, M., and Mishima, T.: Mid-depth circulation in the northwest Pacific during the last deglaciation: Evidence from foraminiferal radiocarbon ages, Geophys. Res. Lett., 30, 2097, doi:10.1029/2003GL018287, 2003.

Altenbach, A. V., Pflaumann, U., Schiebel, R., Thies, A., Timm, S., and Trauth, M.: Scaling percentages and distributional patterns of benthic Foraminifera with flux rates of organic carbon, J. Foraminiferal Res., 29, 173–185, 1999.

Amano, A. and Itaki, T.: Spatial and temporal variation of sedimentation rate and its controlling factors in the Okinawa trough and around the Nansei Islands, Chikyu Monthly, 34, 355–362, 2012.

Amano, A. and Itaki, T.: Variations in sedimentary environments in the forearc and backarc regions of the Ryukyu Arc since 25 kyr based on CNS analysis of sediment cores, submitted, 2015.

Barker, S., Greaves, M., and Elderfield, H.:A study of cleaning procedures used for foraminiferal Mg / Ca paleothermometry, Geochem. Geophys. Geosyst., 4, 8407, doi:10.1029/2003GC000559, 2003.

Behl, R. J. and Kennett, J. P.: Brief interstadial events in the Santa Barbara Basin, NE Pacific, during the past 60 kyr, Nature, 379, 243–246, doi:10.1038/379243a0, 1996.

Bertram, C. J., Elderfield, H., Shackleton, N. J., and Macdonald, J. A.: Cadmium/calcium and carbon isotope reconstructions of the glacial Northeast Atlantic Ocean, Paleoceanogr., 10, 563–578, 1995.

Billups, K. and Schrag, D. P.: Paleotemperatures and ice volume of the past 27 Myr revisited with paired Mg / Ca and $^{18}O/^{16}O$ measurements on benthic foraminifera, Paleoceanogr., 17, PA1003, doi:10.1029/2000PA000567, 2002.

Bingham, F. M. and Lukas, R.: The distribution of intermediate water in the western equatorial Pacific during January–February 1986, Deep-Sea Res., 42, 1545–1573, 1995.

Bostock, H. C., Opdyke, B. N., and Williams, M. J. M.: Characterizing the intermediate depth waters of the Pacific Ocean using $\delta^{13}C$ and other geochemical tracers, Deep-Sea Res. Pt. I, 57, 847–859, 2010.

Boyle, E. A.: Manganese carbonate overgrowths on foraminiferal tests, Geochim. Cosmochim. Acta, 47, 1815–1819, 1983.

Boyle, E. A.: Acomparison of carbon isotopes and cadmium in the modern and glacial maximum ocean: Can we account for the discrepancies? in Carbon Cycling in the Global Ocean: Constrains on the Ocean's role in Global Change, edited by: Zahn, R., Pedersen, T. F., Kaminski, M. A, and Labeyrie, L., Springer-Verlag, New York, 167–194, 1994.

Boyle, E. A. and Keigwin, L. D.: Comparison of Atlantic and Pacific paleochemical records for the last 215 000 years: changes in deep ocean circulation and chemical inventories, Earth Planet. Sci. Lett., 76, 135–150, 1985.

Broecker, W. and Peng, T. H.: Tracers in the Sea, Eldigio Press, New York, 1982.

Broecker, W., Barker, S., Clark, E., Hajdas, I., Bonani, G., and Stott, L.: Ventilation of the glacial deep Pacific Ocean, Science, 306, 1169–1172, 2004.

Broecker, W., Clark, E., and Barker, S.: Near constancy of the Pacific Ocean surface to mid-depth radiocarbon-age difference over the last 20 kyr, Earth Planet. Sci. Lett., 274, 322–326, 2008.

Chikamoto, M., Menviel, L., Abe-Ouchi, A., Ohgaito, R., Timmermann, A., Okazaki, Y., Harada, N., Oka, A., and Mouchet, A.: Variability in North Pacific intermediate and deep water ventilation during Heinrich events in two coupled climate models, Deep-Sea Res. Pt. II, 61–64, 114–126, 2012.

Dickson, A. G.: Thermodynamics of the dissociation of boric-acid in synthetic seawater from 273.15 K to 318.15 K, Deep-Sea Res., 37, 755–766, 1990.

Dickson, A. G. and Millero, F. J.: A comparison of the equilibrium constants for the dissociation of carbonic acid in seawater media, Deep-Sea Res., 34, 1733–1743, 1987.

Duplessy, J. C., Shackleton, N. J., Fairbanks, R. G., Labeyrie, L., Oppo, D., and Kallel, N.: Deepwater source variations during the last climatic cycle and their impact on the global deepwater circulation, Paleoceanogr., 3, 343–360, 1988.

Elderfield, H., Yu, J., Anand, P., Kiefer, T., and Nyland, B.: Calibration for benthic foraminiferal Mg / Ca paleothermometry and the carbonate ion hypothesis, Earth Planet. Sci. Lett., 250, 633–649, 2006.

Elderfield, H., Ferretti, P., Greaves, M., Crowhurst,S., McCave, I. N., Hodell, D., and Piotrowski, A. M.: Evolution of Ocean Temperature and Ice Volume Through the Mid-Pleistocene Climate Transition, Science, 337, 704–709, doi:10.1126/science.1221294, 2012.

Fukasawa, M., Kawano, T., Murata, A., Shibata, F., Kitada, M., Ohama, T., and Ishikawa, Y.: Carbon Dioxide, Hydrographic, and Chemical Data Obtained During the R/V Mirai Repeat Hydrography Cruise in the Pacific Ocean: CLIVAR CO2 Section P10_2005 (25 May–2 July, 2005), http://cdiac.ornl.gov/ftp/oceans/CLIVAR/P10_2005.data/, last access: 7 May 2015, Carbon Dioxide Information Analysis Center, Oak Ridge National Laboratory, US Department of Energy, Oak Ridge, Tennessee, USA, doi:10.3334/CDIAC/otg.CLIVAR_P10_2005, 2005.

Graham, D. W., Corliss, B. H., Bender, M. L., and Keigwin, L. D.: Carbon and oxygen isotopic disequilibria of recent deep-sea benthic foraminifera, Mar. Micropaleontol., 6, 483–497, 1981.

Hanawa, K. and Talley, L.D.: Mode waters. In: Siedler, G., Church, J., Gould, J. (Eds.): Ocean Circulation and Climate: Observing and Modelling the Global Ocean, Academic Press, New York, USA, 373–386 pp., 2001.

Harada, N., Ahagon, N., Sakamoto, T., Uchida, M., Ikehara, M., and Shibata, Y.: Rapid fluctuation of alkenone temperature in the southwestern Okhotsk Sea during the past 120 ky, Global Planet. Change, 53, 29–46, 2006.

Hayward, B. W., Grenfell, H. R., Sabaa, A. T., Neil, H. N., Buzas M. A.: Recent New Zealand deep-water benthic foraminifera, taxonomy, ecologic distribution, biogeography, and use in paleoenvironmental assessment, Science Monographs, N. Z. Geol. Surv. Paleontol. Bull., 77, 1–363, 2010.

Healey, S. L., Thunell, R. C., and Corliss, B. H.: The Mg / Ca-temperature relationship of benthic foraminiferal calcite: New core-top calibrations in the b4 °C temperature range, Earth Planet. Sci. Lett., 272, 523–530, 2008.

Hendy, I. L. and Pedersen, T. F.: Is pore water oxygen content decoupled from productivity on the California Margin? Trace element results from Ocean Drilling Program Hole 1017E, San Lucia slope, California, Paleoceanogr., 20, PA4026, doi:10.1029/2004PA001123, 2005.

Holbourn, A., Henderson, A. S., Macleod, N.: Atlas of Benthic Foraminifera, 1–642, 2013.

Horikawa, K., Asahara, Y., Yamamoto, K., and Okazaki, Y.: Intermediate water formation in the Bering Sea during glacial periods: Evidence from neodymium isotope ratios, Geol., 38, 435–438, 2010.

Hut, G.: Consultants group meeting on stable isotope reference samples for geochemical and hydrological investigations Rep. to Dir. Gen., Int. At. Energy Agency, Vienna, 42 pp., 1987.

Itaki, T.: Preliminary report on radiocarbon ages and radiolarian fossils in core GH08-2004 obtained from east off the Okinawa Island, the western Philippine Sea, GSJ Interim report, 51, 171–175, 2010 (in Japanese).

Itaki, T., Katayama, H., Ikehara, K., Suzuki, A., Kaneko, N., Kawamura, N., and Geshi, N.: Bottomo Sediments in east off the Okinawa main island, GSJ Interim report, 46, 47–65, 2009a (in Japanese).

Itaki, T., Katayama, H., Ikehara, K., Suzuki, A., Kawamura, and N., Sato, K.: Oceanographic conditions in east off the Okinawa main island, GSJ Interim report, 46, 66–77, 2009b (in Japanese).

Itaki, T., Katayama, H., Ikehara, K., Suzuki, A., Kaneko, N., Oda, K., and Arai, K.: Bottom sediments in west off the Okinawa main island, GSJ Interim report, 51, 54–68, 2010 (in Japanese).

Itaki, T., Amano, A., Katayama, H., Suzuki, A., Kaneko, Nishida, N., Shimamura, M., Lee, S., and K., and Arai, K.: Bottom sediments in west off the Okinawa main island (around Kume-Zima and Kerama islands), GSJ Interim report, 55, 57–67, 2011a (in Japanese).

Itaki, T., Amano, A., Katayama, H., and Ikehara, K.: Sediemnt cores in west off the Okinawa main island and their radiocarbon ages, GSJ Interim report, 55, 76–84, 2011b (in Japanese).

Jaccard, S. L. and Galbraith, E. D.: Direct ventilation of the North Pacific did not reach the deep ocean during the last deglaciation, Geophys. Res. Lett., 40, 199–203, doi:10.1029/2012GL054118, 2013.

Kaneko, I., Takatsuki, Y., and Kamiya, H.: Circulation of Intermediate and Deep Waters in the Philippine Sea, J. Oceanogr., 57, 397–420, 2001.

Keigwin, L. D.: Glacial-age hydrography of the far northwest Pacific, Paleoceanogr., 13, 323–339, 1998.

Keigwin, L. D. and Jones, G. A.: Deglacial climate oscillations in the Gulf of California, Paleoceanogr., 5, 1009–1023, doi:10.1029/PA005i006p01009, 1990.

Key, R. M., Kozyr, A., Sabine, C. L., Lee, K., Wanninkhof, R., Bullister, J. L., Feely, R. A., Millero, F. J., Mordy, C., and Peng, T.-H.: A global ocean carbon climatology: Results from Global Data Analysis Project (GLODAP), Global Biogeochem. Cy., 18, GB4031, doi:10.1029/2004GB002247, 2004.

Kitagawa, H., Fukusawa, H., Nakamura, T., Okamura, M., Takemura, K., Hayashida, A. and Yasuda, Y.: AMS ^{14}C dating of varved sediments from Lake Suigetsu, central Japan and atmospheric ^{14}C change during the late Pleistocene, edited by: Cook, G. T., Harkness, D. D., Miller, B. F., and Scott, E. M., Proceedings of the 15th International ^{14}C Conference, Radiocarbon, 37, 371–378, 1995.

Kitani, K.: An oceanographic study of the Okhotsk Sea-particularly in regard to cold waters, Bull. Far Sea Fish. Res. Lab., 9, 45–77, 1973.

Komatsu, K., Hiroe, Y., Yasuda, I., Kawasaki, K., Joyce, T. M. and Bahr, F.: Hydrographic structure and transport of intermediate water in the Kuroshio region off the Boso Peninsula, Japan, J. Oceanogr., 60, 487–503, 2004.

Kroopnick, P.: The distribution of carbon-13 in the world oceans, Deep-Sea Res., 32, 57–84, 1985.

Ku, T.-L. and Oba, T.: A method of quantitative evaluation of calcite dissolution in deep sea sediments and its application to paleoceanographic reconstruction, Quat. Res., 10, 112–129, 1978.

Kubota, Y., Kimoto, K., Tada, R., Oda, H., Yokoyama, Y., and Matsuzaki, H.: Variations of East Asian summer monsoon since the last deglaciation based on Mg/Ca and oxygen isotope of planktic foraminifera in the northern East China Sea, Paleoceanography, 25, PA4205, doi:10.1029/2009PA001891, 2010.

Lear, C. H., Rosenthal, Y., and Slowey, N.: Benthic foraminiferal Mg / Ca paleothermometry: a revised core-top calibration, Geochim. Cosmochim. Acta, 66, 3375–3387, 2002.

Lee, K. E., Lee, H. J., Park, J.-H., Chang, Y.-P., Ikehara, K., Itaki, T., and Kwon, H. K.: Stability of the Kuroshio path with respect to glacial sea level lowering, Geophys. Res. Lett., 40, 1–5, doi:10.1012/grl.50102, 2013.

Locarnini, R. A., Mishonov, A. V., Antonov, J. I. , Boyer, T. P., Garcia, H. E., Baranova, O. K., Zweng, M. M., Paver, C. R., Reagan, J. R., Johnson, D. R., Hamilton, M., and Seidov, D.: World Ocean Atlas 2013, Volume 1: Temperature, edited by: Levitus, S. and Mishonov, A., NOAA Atlas NESDIS 73, 40 pp., 2013.

Lutze, G. F. and Thiel, H.: Epibenthic foraminifera from elevated microhabitats: *Cibicidoides wuellerstorfi* and *Planulina arminensis*, J. Foraminiferal Res., 19, 153–158, 1989.

Martin, P. A., Lea, D. W., Rosenthal, Y., Shackleton, N. J., Sarnthein, M., and Papenfuss, T.: Quaternary deep sea temperature histories derived from benthic foraminiferal Mg / Ca, Earth Planet. Sci. Lett., 222, 275–283, 2002.

Marchitto, T. M., Bryan, S. P., Curry, W. B., and McCorkle, D. C.: Mg / Ca temperature calibration for the benthic foraminifer *Cibicidoides pachyderma*, Paleoceanogr., 22, PA1203, doi:10.1029/2006PA001287, 2007.

Matsumoto, K., Oba, T., Lynch-Stieglitz, J., and Yamamoto, H.: Interior hydrography and circulation of the glacial Pacific Ocean, Quat. Sci. Rev., 21, 1693–1704, 2002.

Max, L., Riethdorf, J.-R., Tiedemann, R., Smirnova, M., Lembke-Jene, L., Fahl, K., Nürnberg, D., Matul, A., and Mollenhauer, G.: Sea surface temperature variability and sea-ice extent in the subarctic northwest Pacific during the past 15 000 years, Paleoceanography, 27, PA3213, doi:10.1029/2012PA002292, 2012.

McCorkle, D. C., Keigwin, L. D., Corliss, B. H., and Emerson, S. R.: The influence of microhabitats on the carbon isotopic composition of deep-sea benthic foraminifera, Paleoceanogr., 5, 161–185, 1990.

McCorkle, D. C., Corliss, B. H., and Farnham, C. A.: Vertical distributions and stable isotopic compositions of live (stained) benthic foraminifera from the North Carolina and California continental margins, Deep-Sea Res., 44, 983–1024, 1997.

Mekik, F. A., Loubere, P. W., and Archer, D. E.: Organic carbon flux and organic carbon to calcite flux ratio recorded in deep-sea carbonates: Demonstration and a new proxy, Global Biogeochem. Cy., 16, 1052, doi:10.1029/2001GB001634, 2002.

Mook, W. G., Bommerson, J. C., and Staverman, W. H., Carbon isotope fractionation between dissolved bicarbonate and gaseous carbon dioxide, Earth Planet. Sci. Lett., 22, 169–176, 1974.

Ogi, M. and Tachibana, Y.: Influence of the annual Arctic Oscillation on the negative correlation between Okhotsk Sea ice and Amur River discharge, Geophys. Res. Lett., 33, L08709, doi:10.1029/2006GL025838, 2006.

Ohkushi, K., Itaki, T., and Nemoto, N.: Last Glacial–Holocene change in intermediate-water ventilation in the Northwestern Pacific, Quat. Sci. Rev., 22, 1477–1484, 2003.

Okazaki, Y., Timmermann, A., Menviel, L., Harada, N., Abe-Ouchi, A., Chikamoto, M. O., Mouchet, A., and Asahi, H.: Deepwater formation in the North Pacific during the last glacial termination, Science, 329, 200–204, 2010.

Okazaki, Y., Sagawa, T., Asahi, H., Horikawa, K., and Onodera, J.: Ventilation changes in the western North Pacific since the last glacial period, Clim. Past, 8, 17–24, doi:10.5194/cp-8-17-2012, 2012.

O'Neil, J. R.: Hydrogen and oxygen isotope fractionation between ice and water, J. Phys. Chemist., 72, 3683–3684, 1968.

O'Neil, J. R., Clayton, R. N., and Mayeda, T. K.: Oxygen isotope fractionation in divalent metal carbonates, J. Chem. Phys., 51, 5547–5558, 1969.

Pelletier, G., Lewis, E., and Wallace, D.: A calculator for the CO_2 system in seawater for Microsoft Excel/VBA, Washington State Department of Ecology, Olympia, WA, Brookhaven National Laboratory, Upton, NY, USA, 2005.

Qu, T. and Lindstrom, E. J.: Northward Intrusion of Antarctic Intermediate Water in the Western Pacific, J. Phys. Oceanogr., 34, 2104–2118, 2004.

Rae, J. W. B., Sarnthein, M., Foster, G. L., Ridgwell, A., Grootes, P. M., and Elliott, T.: Deep water formation in the North Pacific and deglacial CO_2 rise, Paleoceanography, 29, 2013PA002570, 2014.

Raitzsch, M., Kuhnert, H., Groeneveld, J., and Bickert, T.: Benthic foraminifer Mg / Ca anomalies in South Atlantic core top sediments and their implications for Paleothermometry, Geochem. Geophys. Geosyst., 9, Q05010, doi:10.1029/2007GC001788, 2008.

Rathburn, A. E. and Corliss, B. H.: The ecology of living (stained) deep-sea benthic foraminifera from the Sulu Sea, Paleoceanogr., 9, 87–150, doi:10.1029/93PA02327, 1994.

Rathburn, A. E. and De Decker, P.: Magnesium and strontium compositions of recent benthic foraminifera from the Coral Sea, Australia and Prydz Bay, Antarctica, Mar. Micropaleontol., 32, 231–248, 1997.

Regenberg, M., Regenberg, A., Garbe-Schönberg, D., and Lea, D. W.: Global dissolution effects on planktonic foraminiferal Mg / Ca ratios controlled by the calcite-saturation state of bottom waters, Paleoceanography, 29, 127–142, doi:10.1002/2013PA002492, 2014.

Reid, J. L.: Intermediate waters of the Pacific Ocean, Johns Hopkins Oceanographic Studies, No. 2, 85 pp., 1965.

Reid, J. L.: On the total geostrophic circulation of the Pacific ocean: Flow patters, tracers, and transports, Prog. Oceanogr., 39, 263–352, 1997.

Reimer, P. J., Baillie, M. G. L., Bard, E., Bayliss, A., Beck, J. W., Blackwell, P. G., Bronk Ramsey, C., Buck, C. E., Burr, G. S.,Edwards, R. L., Friedrich, M., Grootes, P. M., Guilderson, T. P., Hajdas, I., Heaton, T. J., Hogg, A. G., Hughen, K. A., Kaiser, K. F., Kromer, B., McCormac, F. G., Manning, S. W., Reimer, R. W., Richards, D. A., Southon, J. R., Talamo, S., Turney, C. S. M., van der Plicht, J., and Weyhenmeyer, C. E.: INTCAL09 and MARINE09 radiocarbon age calibration curves, 0–50 000 years cal BP, Radiocarbon, 51, 1111–1150, 2009.

Rella, S. F. and Uchida, M.: A Southern Ocean trigger for Northwest Pacific ventilation during the Holocene?, Scientific Reports, 4, 4046, doi:10.1038/srep04046, 2014.

Rella, S. F., Tada, R., Nagashima, K., Ikehara, M., Itaki, T., Ohkushi, K., Sakamoto, T., Harada, N., and Uchida, M.: Abrupt changes of intermediate water properties on the northeastern slope of the Bering Sea during the last glacial and deglacial period, Paleoceanogr., 27, PA3203, doi:10.1029/2011PA002205, 2012.

Roche, D., Paillard, D., Ganopolski, A., and Hofmann G.: Oceanic oxygen-18 at the present day and LGM: equilibrium simulations with a coupled climate model of intermediate complexity, Earth Planet. Sci. Lett., 218, 317–330, 2004.

Rosenthal, Y., Boyle, E. A., and Slowey, N.: Temperature control on the incorporation of magnesium, strontium, fluorine, and cadmium into benthic foraminiferal shells from Little Bahamas Bank: Prospects for thermocline paleoceanography, Geochim. Cosmochim. Acta, 61, 3633–3643, 1997.

Russell, A. D., Emerson, S., Mix, A. C., and Peterson, L. C.: The use of foraminiferal uranium/calcium ratios as an indicator of changes in seawater uranium content, Paleoceanogr., 11, 649–663, 1994.

Sagawa, T. and Ikehara, K.: Intermediate water ventilation change in the subarctic northwest Pacific during the last deglaciation, Geophys. Res. Lett., 35, L24702, doi:10.1029/2008GL035133, 2008.

Sarnthein, M., Schneider, B., and Grootes, P. M.: Peak glacial ^{14}C ventilation ages suggest major draw-down of carbon into the abyssal ocean, Clim. Past, 9, 2595–2614, doi:10.5194/cp-9-2595-2013, 2013.

Schmidt, G. A., Bigg, G. R., and Rohling, E. J.: Global Seawater Oxygen-18 Database – v1.21, available at: http://data.giss.nasa.gov/o18data/ (last access: 7 May 2015), 1999.

Schmittner, A.: Marine nutrient cycling – How will the ocean's capacity of biological carbon pumping change?, PAGES news, 20, p. 17, 2012.

Schmitz, W. J.: On the world ocean circulation: Volume II, The Pacific and Indian Ocean/A Global Update, Woods Hole Oceanographic Institution, Woods Hole, MA, USA, 237 pp., 1996.

Schlitzer, R.: OceanDataViewSoftware, available at: http://odv.awi.de/ (last access: 7 May 2015), 2009.

Schrag, D. P., Adkins, J. F., McIntyre, K., Alexander, J. L., Hodell, D. A., Charles, C. D., and McManus, J. F.: The oxygen isotopic composition of seawater during the Last Glacial Maximum, Quat. Sci. Rev., 21, 331–342, 2002.

Seki, O., Kawamura, K., Ikehara, M., Nakatsuka, T., and Oba, T.: Variation of alkenone sea surface temperature in the Sea of Okhotsk over the last 85 kyrs, Org. Geochem., 35, 347–354, 2004.

Shackleton, N. J.: Attainment of isotopic equilibrium between ocean water and the benthonic foraminifera genus *Uvigerina*: isotopic changes in the ocean during the last glacial, Centre National de la Recherche Scientifique, Coll. Inter, 219, 203–209, 1974.

Shackleton, N. J., Hall, M. A., and Boersma, A.: Oxygen and carbon isotope data from Leg 74 foraminifers, DSDP Init. Repts., 74, 599–612, 1984.

Sharp, Z.: Principles of Stable Isotope Geochemistry, Pearson Education Inc., Upper Saddle River, NJ, USA, 344 pp., 2007.

Sigman, D. M. and Boyle, E. A.: Glacial/interglacial variations in atmospheric carbon dioxide, Nature, 407, 859–869, 2000.

Stommel, H.: Thermohaline convection with two stable regimes of flow, Tellus, 13, 224–230, 1961.

Stuiver, M. and Reimer, P. J.: Extended ^{14}C database and revised CALIB radiocarbon calibration program, Radiocarbon, 35, 215–230, 1993.

Suzuki, A., Kawamura, N., Itaki, T., Katayama, H., Murayama, S., Usami, T., and Kuroyanagi, A.: Geochemical analyses on sweater samples collected during the GH08 cruise in the eastern offshore of Okinawa Island, GSJ Interim Report, 46, 78–83, 2009. (in Japanese)

Suzuki, A., Ushie, H., Shinmen, K., Amano, A., Kaneko, N., Itaki, T., Katayama, H., Inamura, A., Yasuda, M., Yoshinaga, Y., Murayama, S., and Udami, T.: Geochemical analyses on seawater samples collected during the GH09 cruise in the western off shore of Okinawa Island, GSJ Interim Report, 51, 76–85, 2010. (in Japanese)

Sverdrup, H., Johnson, M. W., and Fleming, R. H.: The Oceans, Their Physics, Chemistry, and General Biology, Prentice-Hall, New York, 1087 pp., 1942.

Tada, R., Sato, S., Irino, T., Matsui, H., and Kennett, J. P.: Millennialscale compositional variations in late Quaternary sediments at Site 1017, Southern California, Proc. Ocean Drill. Program, Sci. Results, 167, 277–296, 2000.

Talley, L. D.: An Okhotsk Sea water anomaly: implications for ventilation in the North Pacific, Deep-Sea Res., 38, S171–S190, 1991.

Talley, L. D.: Distribution and Formation of North Pacific Intermediate Water, J. Phys. Oceanogr., 23, 517–537, 1993.

Talley, L.D.: Antarctic Intermediate Water in the South Atlantic, The South Atlantic: Present and Past Circulation, 219–238, 1996.

Tisserand, A. A., Dokken, T. M., Waelbroeck, C., Gherardi J.-M., Scao, V., Fontanier, C., and Jorissen, F.: Refining benthic foraminiferal Mg / Ca-temperature calibrations using core-tops from the western tropical Atlantic: Implication for paleotemperature estimation, Geochem. Geophys. Geosyst., 14, 929–946, doi:10.1002/ggge.20043, 2013.

Toyofuku, T., Kitazato, H., Kawahata, H., Tsuchiya, M., and Nohara, M.: Evaluation of Mg / Ca thermometry in foraminifera: Comparison of experimental results and measurements in nature, Paleoceanogr., 15, 456–464, 2000.

Tsuchiya, M. and Talley, L.D.:A Pacific hydrographic section at 881W: water property distribution, J. Geophys. Res., 103, 12899–12918, 1998.

Waelbroeck, C., Labeyrie, L., Michel, E., Duplessy, J. C., McManus, J. F., Lambeck, K., Balbon, E., and Labracherie, M.: Sea level and deep water temperature changes derived from ben-

thic foraminifera isotopic records, Quat. Sci. Rev., 21, 295–305, doi:10.1016/S0277-3791(01)00101-9, 2002.

Wan, S. and Jian, Z.: Deep water exchanges between the South China Sea and the Pacific since the last glacial period, Paleoceanography, 29, 1162–1178, 2014.

Warren, B. A.: Why is no deep water formed in the North Pacific, J. Mar. Res., 41, 327–347, doi:10.1357/002224083788520207, 1983.

Yasuda, I.: The origin of the North Pacific Intermediate Water, J. Geophys. Res., 102, 893–909, 1997.

Yasuda, I.: North Pacific Intermediate Water: progress in SAGE (Subarctic Gyre Experiment) and related projects, J. Oceanogr., 60, 385–395, 2004.

Yoneda, M., Uno, H., Shibata, Y., Suzuki, R., Kumamoto, Y., Yoshida, K., Sasaki, T., Suzuki, A., and Kawahata, H.: Radiocarbon marine reservoir ages in the western Pacific estimated by pre-bomb molluscan shells, Nucl. Instr. Meth. B, 259, 432–437, 2007.

Yu, J. and Elderfield, H.: Mg / Ca in the benthic foraminifera Cibicidoides wuellerstorfi and Cibicidoides mundulus: Temperature vs. carbonate ion saturation, Earth Planet Sci. Lett., 276, 129–139, 2008.

Yu, J., Anderson, R. F., and Rohling, E. J.: Deep Ocean Carbonate Chemistry and Glacial-Interglacial Atmospheric CO_2 Changes, Oceanogr., 27, 16–25, doi:10.5670/oceanog.2014.04, 2014.

Zweng, M. M, Reagan, J. R., Antonov, J. I., Locarnini, R. A., Mishonov, A. V., Boyer, T. P., Garcia, H. E., Baranova, O. K., Johnson, D. R., Seidov, D., and Biddle, M. M.: World Ocean Atlas 2013, Volume 2: Salinity, edited by: Levitus, S. and Mishonov, A., NOAA Atlas NESDIS 74, 39 pp., 2013.